Bone marrow age dictates clonality of smooth muscle-derived cells in the atherosclerotic plaque

Inamul Kabir[1,2], Xinbo Zhang[3], Jui Dave[1,2], Raja Chakraborty[1], Rihao Qu[4], Rachana R. Chandran[1,2], Aglaia Ntokou[1,2], Binod Aryal[3], Noemi Rotllan[3], Rolando Garcia-Milian[5], John Hwa[1], Yuval Kluger[4], Kathleen A. Martin[1], Carlos Fernández-Hernando[3,4] and Daniel M. Greif[1,2]*

[1]Yale Cardiovascular Research Center, Section of Cardiovascular Medicine, Department of Internal Medicine, Departments of [2]Genetics, [3]Comparative Medicine and [4]Pathology, [5]Bioinformatics Support Program Yale University, New Haven, CT 06511, USA

*To whom correspondence should be addressed: daniel.greif@yale.edu, 203-737-2040 (phone), 203-737-6118 (FAX)

Conflict of interest: The authors have declared that no conflict of interest exists.

Abstract

Aging is the predominant risk factor for atherosclerosis, the leading cause of death. Rare smooth muscle cells (SMCs) clonally expand giving rise to up to ~70% of atherosclerotic plaque cells; however, the effect of age on SMC clonality is not known. Our results indicate that aging induces SMC polyclonality and worsens atherosclerosis through non-cell autonomous effects of aged bone marrow-derived cells. Indeed, in myeloid cells from aged mice and humans, TET2 levels are reduced which epigenetically silences integrin β3 resulting in increased cytokine (e.g., tumor necrosis factor [TNF]-α) signaling. In turn, TNFα induces recruitment and expansion of multiple SMCs into the atherosclerotic plaque. Recent studies demonstrate that normal aging is characterized by somatic mutations and clonal expansion of epithelial cells of diverse tissues (e.g., esophagus, endometrium, skin); extrapolating beyond atherogenesis, our results call for future studies evaluating the role of aged myeloid cells in regulating this epithelial cell clonal expansion.

Keywords

Atherosclerosis, atheroma, aging, smooth muscle cells, clonality, integrin β3, macrophages, inflammation.

Introduction

The revolution of single cell transcriptomics has unveiled a wealth of heterogeneity within populations of specific cell types. On the other hand, clonal expansion of individual cells is increasingly appreciated to underlie a number of diseases in addition to cancer, including vascular pathologies, cirrhosis, and neurodegeneration[1-6]. For instance, multiple smooth muscle cell (SMC) progenitors give rise to the normal arterial wall during development, but a select few progenitors within the wall participate in atherosclerotic plaque formation[2-4,7]. Additionally, in age-related clonal hematopoiesis of indeterminate potential (CHIP), stem cells carrying somatic mutations give rise to dominant leukocyte variants, and CHIP is associated with an increased risk of major atherosclerosis-related cardiovascular diseases, myocardial infarction and ischemic stroke[8,9]. Recent studies provide evidence for a similar progressive accumulation of mutated somatic clones in epithelial cells of the normal esophagus, endometrium, skin and bronchi of aging humans[10-13]. Investigations have primarily focused on cell autonomous mechanisms underlying clonal expansion, and non-cell autonomous regulation of clonality is not well understood, particularly in the context of aging. Of note, a recent controversial bioinformatic study challenges the view that increasing somatic mutations with age underlies the enhanced incidence of cancer later in life and instead argues that age-induced decline of the immune system is paramount[14,15]. Herein, we aim to investigate the phenomenon of non-cell autonomous regulation of clonality in aging by delineating the role of aged hematopoietic cells in modulating SMC recruitment and clonal expansion in the atherosclerotic plaque.

Aging is the dominant risk factor for atherosclerosis, which underlies myocardial infarction and stroke and thus, is the leading cause of death globally[16]. Inflammatory cells, especially macrophages, and SMCs are key players in atherosclerotic plaques. In response to

sub-endothelial lipid accumulation and inflammation, rare SMC progenitors from the tunica media contribute cells that populate the nascent plaque. As the lesion progresses, this lineage clonally expands giving rise to ~30-70% of the total cellularity of an advanced plaque with cells forming the protective fibrous cap or transitioning into plaque destabilizing fates[2-4,17-19]. Integrins are heterodimeric proteins that link the extracellular and intracellular compartments, and transplant of bone marrow (BM) null for the gene encoding integrin β3 (*Itgb3*) in atheroprone mice induces multiple SMC progenitors to enter the plaque and clonally expand, exacerbating disease burden[2,20]. On an *Apoe*$^{(-/-)}$ background, BM-derived macrophages that are null for *Itgb3* have elevated levels of the cytokine tumor necrosis factor (TNF)-α[20]. Plasma TNFα levels are increased in aged mice and humans, and high TNFα levels in older humans are correlated with atherosclerosis[21,22]. Importantly, BM transplant (BMT) from aged mice into young mice worsens atherosclerosis[23], but underlying mechanisms and especially, effects on SMC recruitment and clonality, are not delineated.

In CHIP, clonally expanded hematopoietic stem cells commonly harbor somatic mutations in epigenetic regulators, such as *Ten Eleven Translocation (TET)-2*[refs. 8,9]. On a *Ldlr*$^{(-/-)}$ background, *Tet2*-deficient BM predisposes mice to develop Western diet (WD)-induced atherosclerosis, and macrophages isolated from *Tet2*$^{(-/-)}$ mice express elevated levels of cytokines, including interleukin (IL)-1β, IL6 and TNFα[9,24]. Macrophages recruited to the atherosclerotic plaque during early stages of disease proliferate locally during plaque progression[25], and in atheroprone mice, initiating WD in the aged as compared to the young increases the accumulation of macrophages in the aorta[23]. Importantly in the context of CHIP in humans or in aged or myeloid cell *Tet2*-deficient mice, the clonality of myeloid cells in the

atherosclerotic plaque itself is elusive. And similar to aging, the effect of BM *Tet2*-deficiency on SMC clonality in the plaque is not delineated.

Herein, we report that the age of the BM is a key factor dictating the clonality of SMC-derived cells in the atherosclerotic plaque: aged BM non-cell autonomously induces recruitment and expansion of multiple SMC progenitors. Mechanistically, reduced TET2 levels in aged monocytes/macrophages epigenetically decreases *Itgb3* gene expression, which enhances cytokine (e.g., TNFα) signaling, and thus, polyclonality of the SMC lineage and worse atherosclerosis ensue.

Results

Age of mice dictates clonality of SMC- and monocyte/macrophage-derived plaque cells.

In the setting of hypercholesterolemia in mice, rare smooth muscle myosin heavy chain $(SMMHC)^{+}$ cells migrate into each atherosclerotic plaque and clonally expand, giving rise to up to two-thirds of the total cells in an advanced plaque[2-4,17,26]. However, the clonality of macrophages in plaques and how aging regulates SMC and macrophage clonality are undefined. (Throughout our studies, young and aged mice refer to 3 and 18 month old mice, respectively.) To this end, young and aged mice carrying one allele of the multi-color *ROSA26R-Rainbow (Rb)* Cre reporter and either *Myh11-CreER*^{T2} or *Csf1r-Mer-iCre-Mer* were induced with tamoxifen (1 mg/day for 5 or 20 days, respectively), rested for 1 week, injected with recombinant adeno-associated virus (AAV) encoding constitutively active PCSK9 ([AAV-*Pcsk9*]; to deplete hepatic LDLR) and after an additional 4 weeks rest, fed a WD for 16 weeks (Fig. 1a). Transverse aortic root sections were subjected to histological staining with H&E or oil red O (ORO) or stained for nuclei (DAPI) and directly imaged for Rb colors (Cerulean [Cer], membrane Cherry [mCh] and

membrane Orange [mOr]). In comparison to atherosclerotic plaques in young mice, plaques in aged mice are larger and have increased lipid content (Fig. 1b-e). Furthermore, the percent of plaque cells that derive from SMCs (i.e., marked by any Rb color) does not change with age, but there is a marked shift towards polyclonality (Fig. 1f-h). Indeed, for young mice, the most prevalent color (#1) in each plaque comprises 97±1% of marked cells, and the second and third most prevalent color (#2, 3) make up the remaining ~3%. For aged mice, the marked cells are substantially more distributed among the Rb colors at 50±5%, 28±4% and 22±6%. Importantly, the distribution of marked cells of the tunica media underlying the plaques are similar in young and aged mice (Fig. 1i). In contrast to these results with SMC tracing, in plaques of aged mice, $CSF1R^{+}$ cells give rise to a ~3-fold higher percentage of cells and are considerably more dominated by a single clone than in plaques of young mice (i.e., 95±3%, 3±1%, 1±1% vs. 63±9%, 25±5%, 12±3%; Fig. 1j-l). Thus, aging induces polyclonality of SMC-derived cells but dominance by a single clone of the monocyte/macrophage lineage in atherosclerotic plaques.

Age of the BM is the key determinant of clonality of SMC-derived cells in the plaque

In atheroprone mice, transplant of aged or *Itgb3*$^{(-/-)}$ BM worsens WD-induced atherosclerosis, and in the latter case, results in the recruitment and expansion of multiple SMCs in the plaque[2,20,23]. We next queried whether aged BM is sufficient to induce polyclonality of SMC-derived plaque cells. To this end, young *Ldlr*$^{(-/-)}$, *Myh11-CreER*^{T2}, *ROSA26R*$^{(Rb/+)}$ recipients were induced with tamoxifen, rested, and transplanted with BM from young and aged wild type donors (Fig. 2a). Four weeks after BMT, engraftment was confirmed (Fig. 2b). After feeding recipients a WD for 16 weeks, mice were euthanized, and transverse aortic root sections were directly imaged for Rb colors (Fig. 2c). The percentage of plaque cells derived from SMCs in

recipients of aged BM is twice that in young BMT recipients (Fig. 2d). Furthermore, labeled plaque cells in recipients of young BM are dominated by a single Rb color: color #1, 2 and 3 in each plaque comprise 95±2%, 4±1% and 2±1%, of marked cells, respectively (Fig. 2e). In stark contrast, labeled plaque cells in recipients of aged BM are much more equally distributed at rates of 37±3%, 34±6% and 29±3%. Importantly, the distribution of marked tunica media cells underlying the plaques are similar in young and aged BMT groups (Fig. 2f). Of note, using a distinct mouse model of high cholesterol-induced atherosclerosis, similar results were obtained in regard to transplant recipients of aged BM having worse atherosclerosis and more equitable color distribution of Rb marked cells of the SMC lineage than with recipients of young BM (Fig. S1a-h). Thus, transplant of aged BM into a young mouse induces polyclonal expansion of multiple SMC progenitors in the atherosclerotic plaque.

For a SMC progenitor to clonally expand in the atherosclerotic plaque, it must migrate into the atheroma and proliferate. Macrophages regulate SMC migration and proliferation[2,27], and thus, we evaluated whether aging influences the effects of macrophages on these processes. Monocytes were harvested from BM of young and aged mice and differentiated into macrophages in culture, and macrophage conditioned medium was collected. SMCs were isolated from the aorta of young mice and incubated with this conditioned medium. SMCs incubated with conditioned medium from aged as opposed to young macrophages for 6 or 8 h induces SMC migration without altering proliferation at 8 h as determined by EdU incorporation (Figs. 2g, h, S1i, j). However, culturing SMCs for 48 h in aged macrophage conditioned medium enhances proliferation by ~3 fold (Fig. 2i, j). In sum, aged BM-derived cells (presumably macrophages) facilitate the recruitment of multiple pre-existing SMCs into the plaques as aged macrophage-derived conditioned medium enhances SMC migration and proliferation.

As a complementary approach, we next evaluated the effect of transplanting a young BM on clonality of SMC-derived plaque cells in an aged recipient. Aged *Myh11-CreER*^{T2}, *ROSA26R*$^{(Rb/+)}$ mice were induced with tamoxifen, rested, transplanted with young and aged BM, injected with AAV-*Pcsk9* and fed a WD for 16 weeks (Fig. S2a). In comparison to aged BMT, young BMT attenuates atherosclerotic lesion burden and lipid deposition as evidenced by staining of transverse aortic root sections with H&E and ORO, respectively (Fig. S2b-e). Furthermore, sections were directly imaged for Rb colors, and with young BMT, the SMC-derived cells make up a smaller percentage of the plaque cells and are dominated by a single clone (Fig. S2f-i). Taking the findings from Figures 1, 2, S1 and S2 together, the age of the BM is a decisive factor determining the clonality of SMC-derived plaque cells.

Tet2 in BM cells regulates clonality of SMC-derived cells in plaques

Loss-of-function mutations in a few genes that encode epigenetic regulators, such as *TET2*, account for the majority of CHIP cases[8]. Transplant of *Tet2* deficient BM to *Ldlr*$^{(-/-)}$ mice exacerbates WD-induced atherosclerosis[9,24]; however, the effect of BM TET2 on SMC clonality is not delineated. Thus, young *Ldlr*$^{(-/-)}$, *Myh11-CreER*^{T2}, *ROSA26R*$^{(Rb/+)}$ recipient mice were induced with tamoxifen, rested, transplanted with *Tet2*$^{(-/-)}$ or wild type BM and fed a WD for 16 weeks (Fig. 3a, b). The percent of atherosclerotic plaque cells that are SMC-derived is enhanced with *Tet2*$^{(-/-)}$ BMT (Fig. 3c, d). Moreover, labeled cells in plaques of the wild type BMT group are dominated by a single Rb color (color #1: 88±3%; #2: 8±3%; #3: 4±1%) in contrast to the more evenly distributed labeling in the *Tet2*$^{(-/-)}$ BMT group (48±3%, 30±4%, 22±3%; Fig. 3e). The color distribution of labeled cells in the underlying tunica media does not differ between the BMT groups (Fig. 3f).

As a more specific evaluation of the role of TET2 in myeloid cells in atherosclerosis, transplant of *LysM-Cre, Tet2*$^{(flox/flox)}$ BM into *Ldlr* null mice has been shown to worsen WD-induced atherosclerosis[9,24]. We next investigated whether medium conditioned by *Tet2*$^{(-/-)}$ macrophages induces SMC migration and proliferation. Monocytes isolated from wild type or *Tet2*$^{(-/-)}$ BM were differentiated into macrophages, and conditioned medium was collected. Migration of isolated murine aortic SMCs is induced by culturing with *Tet2*$^{(-/-)}$ macrophage conditioned medium for 6 or 8 h whereas proliferation is not affected at 8 h (Figs. 3g, h, S1k, l). However, culturing in *Tet2*$^{(-/-)}$ macrophage conditioned medium for 48 h increases SMC proliferation by ~3 fold in comparison to culturing in wild type conditioned medium (Fig. 3i, j). Thus, akin to the results with aged BM, *Tet2*$^{(-/-)}$ BM-derived cells (most likely macrophages) facilitate the recruitment and polyclonal expansion of multiple pre-existing SMCs into the plaque.

In BM-derived monocytes, reduced TET2 is a link between aging and reduced integrin β3

To begin to evaluate how aged BM cells exacerbate atherosclerosis and induce SMC recruitment/expansion in the plaque, we investigated the effects of age on the murine and human monocyte transcriptome. $CD3^{-}CD19^{-}Cd11b^{+}Ly6C^{+}$ monocytes were isolated from the BM of young and aged mice by flow-activated cell sorting (FACS) and subjected to bulk RNA-sequencing (seq) (Dataset S1) and pathway analysis. Gene Set Enrichment Analysis (GSEA) indicates that inflammatory and immune pathways are upregulated in aged monocytes (Fig. 4a). An overrepresentation analysis in IPA showed that atherosclerosis is one of the top overrepresented and activated diseases/functions ($p = 6.06 \times 10^{-38}$, z-score = 0.65). In addition, 20 differentially expressed genes significantly overlap with atherosclerosis in the Ingenuity

Knowledge Base ($p = 7.52 \times 10^{-23}$; Fig. 4b). Notably, Itgb3 is downregulated in aged monocytes (Fig. 4b), and we and others have previously demonstrated that in atheroprone mice, *Itgb3*$^{(-/-)}$ BMT exacerbates atherosclerosis and induces polyclonal expansion of SMC progenitors in the plaque[2,20]. However, a link between integrin β3 deficiency in monocytes/macrophages and aging has not previously been established.

We next further explored this potential link by directly evaluating specific gene product levels in monocytes/macrophages from mice and humans. BM was harvested from young and aged mice, and we either isolated monocytes by FACS or differentiated them into macrophages in culture. Additionally, FACS was used to isolate peripheral blood $CD3^{-}CD19^{-}CD14^{+}$ monocytes from healthy young and older humans (25±3 yr and 55±7 yr, respectively; Table S1). qRT-PCR of monocyte lysates demonstrate substantially reduced ITGB3 mRNA levels in aged mice and humans (Fig. 4c, d). Furthermore, in comparison to young macrophages, aged macrophages have a 75±19% reduction in integrin β3 protein levels but similar levels of the monocyte/macrophage marker CSF1R (Fig. 4e, f).

We then queried whether Itgb3 levels are modulated by TET2 which catalyzes the oxidation of 5-methylcytosine (5mC) to 5-hydroxymethylcytosine (5hmC), a key step during DNA demethylation and thus, gene expression. Our data indicate that monocytes from aged mice have reduced TET2 protein levels and that 5hmC levels in proximity to the *ITGB3* transcription start site in aged human and murine monocytes are decreased (Fig. 4g-j). Similarly, monocytes isolated from *Tet2*$^{(-/-)}$ mice have reduced 5hmC levels at the *Itgb3* proximal promoter and reduced Itgb3 transcript levels (Fig. 4k, l). Hence, the data suggest that reduced TET2 in aged monocytes leads to reduced ITGB3 levels by attenuating transcription.

Itgb3 deficient monocytes/macrophages exacerbate atherosclerosis and clonally expand in the plaque

Although transplant of atheroprone mice with *Itgb3*$^{(-/-)}$ BM worsens diet-induced atherosclerosis[2,20], the *in vivo* role of integrin β3 in myeloid cells has not been elucidated. *Apoe*$^{(-/-)}$*, Csf1r-Mer-iCre-Mer* mice carrying *Itgb3*$^{(flox/flox)}$ or *Itgb3*$^{(+/+)}$ were induced with tamoxifen (1 mg/day for 20 days), rested and fed a WD for 16 weeks. Deletion of *Itgb3* in CSF1R^{+} cells exacerbates aortic root plaque burden, lipid accumulation and acellular necrotic core area (Figs. 5a-d, S3a, b).

We next studied mice of the same genotypes and additionally with *ROSA26R*$^{(mTmG/+)}$ or *ROSA26R*$^{(Rb/+)}$. Five days after tamoxifen induction of *Apoe*$^{(-/-)}$*, Csf1r-Mer-iCre-Mer, ROSA26R*$^{(mTmG/+)}$ mice also carrying *Itgb3*$^{(flox/flox)}$ or *Itgb3*$^{(+/+)}$, cells expressing GFP and the monocyte marker Ly6C were isolated from BM by FACS and peripheral blood was collected as well. qRT-PCR analysis of Ly6C^{+}GFP^{+} BM cells demonstrated a 94±4% reduction in Itgb3 levels in mice carrying *Itgb3*$^{(flox/flox)}$ (Fig. S3c). Deletion of *Itgb3* in CSF1R^{+} cells does not alter circulating levels of total cholesterol, triglycerides or leukocyte sub-types (Fig. S3d-f). To evaluate the fate and proliferation of the lineage derived from CSF1R^{+} cells, following tamoxifen induction, mice of these same genotypes were fed a WD for 16 weeks and then injected with EdU intraperitoneally 12 h prior to euthanasia. Transverse aortic root sections were stained for GFP, α-smooth muscle actin (SMA) and either EdU or the macrophage marker CD68 (Figs. 5e, S3g). *Csf1r-Mer-iCre-Mer*-mediated deletion of *Itgb3* leads to proliferation and accumulation of cells of this lineage in the plaque as well as an increased percentage of total plaque cells that are CD68^{+} (Figs. 5f, S3h, i). Given that CSF1R^{+} cells clonally expand in the plaques of aged mice (see Fig. 1j-l) and the link between aging and monocyte/macrophage Itgb3 deficiency (see Fig.

4), we next queried whether CSF1R^{+} cells deficient in *Itgb3* clonally expand. *Apoe$^{(-/-)}$, Csf1r-Mer-iCre-Mer, ROSA26R$^{(Rb/+)}$* mice also harboring *Itgb3$^{(flox/flox)}$* or *Itgb3$^{(+/+)}$* were induced with tamoxifen, rested and then fed a WD for 6 or 9 weeks. Aortic root sections were stained with DAPI and directly imaged for the Rb colors (Fig. 5g). For plaques in mice carrying *Itgb3$^{(flox/flox)}$*, a higher percentage of cells derive from the CSF1R^{+} lineage and a single Rb color gives rise to ~90% of marked cells at each WD duration, whereas in mice wild type for *Itgb3*, there is a more equitable distribution of the three Rb colors (Fig. 5h, i). Taken together, integrin β3 deficiency in monocytes/macrophages leads to clonal expansion of this population in the atherosclerotic plaque and more severe disease.

Itgb3 deficient SMCs contribute less to the plaque and attenuate atherosclerosis

In addition to myeloid cells, SMCs express high levels of integrin β3, and on an atheroprone background, global *Itgb3* deletion exacerbates atherosclerosis[2]; however, in this context, the cell autonomous role of integrin β3 in SMC-derived cells is not defined. *Apoe$^{(-/-)}$, Myh11-CreER^{T2}* mice also carrying *Itgb3$^{(flox/flox)}$* or *Itgb3$^{(+/+)}$* and *ROSA26R$^{(mTmG/+)}$* or *ROSA26R$^{(Rb/+)}$* were induced with tamoxifen (1 mg/day for 5 days), rested and then fed a WD for 16 weeks. The aortic root of the *Itgb3$^{(flox/flox)}$* mice have reduced plaque burden, lipid accumulation and necrotic core area (Fig. S4a-e). Prior to investigating the effect of *Itgb3* deletion on the SMC lineage during atherogenesis, *Apoe$^{(-/-)}$, Myh11-CreER^{T2}*, *ROSA26R$^{(mTmG/+)}$* mice also carrying *Itgb3$^{(flox/flox)}$* or *Itgb3$^{(+/+)}$* were induced with tamoxifen and rested and then peripheral blood was collected and aortic GFP^{+} cells (i.e., SMCs) were isolated by FACS. Efficient *Itgb3* deletion (92±6% reduction in transcript levels) in GFP^{+} SMCs of *Itgb3$^{(flox/flox)}$* mice was confirmed (Fig. S4f). Total cholesterol and triglyceride levels did not differ between

genotypes (Fig. S4g, h). To trace the SMC lineage, after inducing with tamoxifen, mice of this genotype were fed a WD for 16 weeks and injected with EdU 12 h prior to euthanasia. Immunohistochemistry of aortic root sections demonstrated a ~2-fold reduction in both proliferation and accumulation of SMC-derived cells in the plaque (Fig. S4i-k). To evaluate clonality, *Apoe*$^{(-/-)}$, *Myh11-CreER*^{T2}, *ROSA26R*$^{(Rb/+)}$ mice also carrying *Itgb3*$^{(flox/flox)}$ or *Itgb3*$^{(+/+)}$ were induced with tamoxifen, rested and fed a WD for 16 weeks. Aortic root sections were stained with DAPI and directly imaged for Rb colors (Fig. S4l). Deletion of *Itgb3* did not alter the distribution of SMC-derived clones in the atherosclerotic plaque or underlying media (Fig. S4m, n).

We next evaluated molecular mechanisms that may link integrin β3 deficiency in SMCs to attenuated atherosclerosis. Signaling pathways mediated by AKT, extracellular regulated kinase (ERK), and p21 activated kinase (PAK)-1 induce SMC proliferation and/or migration[28-31]. Herein, aortas were harvested from wild type and *Itgb3*$^{(-/-)}$ mice, and Western blots of homogenates indicate a 72±7% reduction in phosphorylated AKT in *Itgb3* nulls (Fig. S5a, b). As an alternative, siRNA targeting of Itgb3 in isolated wild type aortic SMCs significantly reduces protein levels of phosphorylated AKT, ERK and PAK-1 (Fig. S5c, d). Moreover, Itgb3 silencing abrogates platelet-derived growth factor-B-induced dorsal ruffle formation (Fig. S5e, f), an early step in cell migration[32]. In sum, SMCs that are deficient in Itgb3 have decreased proliferation and migration, which likely accounts for their reduced contribution to the atherosclerotic plaque.

Itgb3$^{(-/-)}$ monocytes/macrophages are pro-inflammatory

While SMC *Itgb3* deletion attenuates atherosclerosis, transplant of *Itgb3*$^{(-/-)}$ BM or deletion of *Itgb3* in monocytes/macrophages exacerbates disease[2,20] (see Figs. 5, S3a, b, S4a-e).

In regard to SMC migration and proliferation, medium conditioned by *Itgb3*$^{(-/-)}$ macrophages is inductive whereas reduction of integrin β3 in SMCs is inhibitory[2] (see Fig. S5). Moreover, *Itgb3*$^{(-/-)}$ BMT results in polyclonal SMC expansion in the plaque, but *Itgb3* deletion in SMCs does not alter cell autonomous clonality[2] (see Fig. S4l-n). Thus, the role of integrin β3 in monocytes/macrophages warrants further investigation. To this end, we performed single cell (sc) RNA-seq in BM cells from *Apoe*$^{(-/-)}$ mice that are also wild type or null for *Itgb3*. Unsupervised clustering was used to generate t-distributed stochastic neighbor embedding (t-SNE) plots, separating the cells into four major cell type groups: neutrophils, monocytes/macrophages, B-cells, T-cells (Figs. 6a, b, S6a). These plots do not clearly identify cell populations that are unique to one of the genotypes nor does the proportion of cell types markedly differ between genotypes (Fig. S6b). Given our focus on monocytes/macrophages, we evaluated the expression pattern of classical markers of these cell types (e.g., Adgre1, Ccr2, Cd68, Csf1r and Cx3cr1; Fig. S6c).

GSEA of *Apoe*$^{(-/-)}$ monocytes/macrophages demonstrates that deletion of *Itgb3* leads to activation of inflammation and the immune system, including pathways involving chemokines, cytokines and cell adhesion molecules (Fig. 6c). More specifically, signaling pathways involving Toll-like receptor, IL17, TNF, and nuclear factor kappa B are upregulated. These results extend a prior study demonstrating that on an *Apoe*$^{(-/-)}$ background, BM-derived macrophages from *Itgb3*$^{(-/-)}$ mice, compared to *Itgb3* wild type mice, have elevated TNFα levels[20]. We evaluated the expression levels of differentially expressed genes in our dataset that are annotated as part of TNF, chemokine or cytokine signaling pathways (Fig. 6d). The vast majority of genes (i.e., 23 of 25) are upregulated in the *Itgb3* null monocytes/macrophages. In addition, IPA of differentially

expressed genes predicts that *Itgb3* deletion induces the inflammatory response and monocyte/macrophage migration and proliferation (Fig. 6e).

TNFα regulates clonal expansion of SMC-derived plaque cells

Treatment with an anti-TNFα antibody prolongs survival of WD fed *Apoe*$^{(-/-)}$ *Itgb3*$^{(-/-)}$ mice[20]; however, effects of TNFα inhibition on atherosclerotic burden are controversial[33,34], and effects on SMC clonality are not defined. To this end, *Apoe*$^{(-/-)}$, *Csf1r-Mer-iCre-Mer, Itgb3*$^{(flox/flox)}$ mice were induced with tamoxifen (1 mg/day, 20 days), rested and injected intraperitoneally with an anti-TNFα neutralizing antibody or IgG2a isotype control twice per week during the 12 weeks of WD feeding (Fig. 7a). TNFα inhibition attenuates plaque area and lipid burden in the aortic root (Fig. 7b-e). For clonal analysis, *Apoe*$^{(-/-)}$, *Myh11-CreER*^{T2}, *ROSA26R*$^{(Rb/+)}$ mice were induced with tamoxifen (1 mg/day, 5 days), rested, transplanted with *Apoe*$^{(-/-)}$ BM that was also wild type or null for *Itgb3* and 4 weeks later, started on a 12 week regimen of WD with concomitant twice weekly injections of anti-TNFα antibody or control IgG2a (Fig. 7f-h). Aortic root sections were stained with DAPI and directly imaged for the Rb colors (Fig. 7i, j). In both *Itgb3* wild type or *Itgb3*$^{(-/-)}$ BMT groups, inhibition of TNFα reduces SMC-derived plaque cells by more than 50% (Fig. 7k). Furthermore, in mice transplanted with the *Itgb3*$^{(-/-)}$ BM, anti-TNFα treatment induces predominance of a single SMC-derived clone (color #1: 87±6%; #2: 10±3%; #3: 3±2%) in comparison to the more evenly distributed polyclonality with IgG2a control (40±4%, 33±2%, 26±3%) (Fig. 7l). Treatment with the anti-TNFα antibody does not alter clonal distribution of SMC-derived cells in either plaques of the *Itgb3*$^{(+/+)}$ BMT group or the underlying media with each BMT group (Fig. 7l, m).

Finally, as aged myeloid cells have reduced integrin β3 levels (see Fig. 4c-f), we assessed the effect of TNFα blockade on SMC clonality in the context of aged BM. Young *Ldlr*$^{(-/-)}$, *Myh11-CreER*^{T2}, *ROSA26R*$^{(Rb/+)}$ mice were induced with tamoxifen, transplanted with BM from aged wild type mice and treated with anti-TNFα antibody or control IgG2a during 12 weeks of WD feeding (Fig. S7a-c). TNFα blockade reduces the contribution of SMC-derived cells to the plaque (Fig. S7d, e). Moreover, anti-TNFα treatment promotes expansion of a single SMC-derived clone (color #1: 86±4%; #2: 11±2%; #3: 3±1%) in comparison to control IgG2a-treated plaques (54±6%, 27±6%, 19±4%) without altering the distribution of SMC clones in the underlying media (Fig. S7d, f, g).

Discussion

The main finding of this work is that the age of the BM non-cell autonomously dictates clonality of SMCs in the atherosclerotic plaque, and this effect is not dependent on the age of SMCs or other non-hematopoietic cells (Figs. 1-3, S1, 2). The normal aging process of many tissues, such as esophagus, endometrium and skin as well as the pathogenesis of major diseases associated with aging (e.g., cancer, atherosclerosis and neurodegeneration) are characterized by expansion of discrete cellular clones[2-5,10-12]. A central tenet of oncogenesis is that the lineage of a founder cell accrues a series of somatic driver mutations over time until growth control is lost, and uncontrolled proliferation ensues[35,36]. In contrast, there is relatively limited understanding of non-cell autonomous regulation of clonal expansion, especially in the context of aging. Taking prior work from our and other groups together, ~30-70% of the cellularity of a given advanced atherosclerotic plaque in a young mouse derives from clonal expansion of one or two SMC progenitors[2-4,17,18,26]. Our results herein indicate that in the plaques of aged mice, this SMC

expansion is instead polyclonal as a result of aged BM-derived cells. This effect is likely in large part due to macrophages as conditioned medium from old macrophages induces SMC proliferation and migration (Fig. 2).

In the vast majority of prior studies of atherosclerosis in aged mice, *Apoe* or *Ldlr* nulls were aged on a chow diet prior to WD feeding; however, these mice develop high cholesterol and atherosclerosis during aging, making it challenging to differentiate the effects of aging from that of prolonged exposure to hypercholesterolemia. To circumvent this issue, our studies of WD-induced atherosclerosis in aged mice primarily utilize AAV-*Pcsk9*, allowing for the separation of the effects of aging and prolonged exposure to hypercholesterolemia[37-39]. Our data with atherogenesis of *Myh11-CreER, ROSA26R*$^{(Rb/+)}$ mice indicate SMC progenitors expand in the plaque in a mono/oligoclonal manner in the young and in a polyclonal fashion in the aged (Fig. 1). Similar to atherogenesis, neointima formation in ligated carotid arteries of young mice is characterized by oligoclonal expansion of rare SMCs[3]. Cellular senescence is a key component of aging; however, in contrast to atherosclerosis in aged mice, telomere damage-induced senescence in SMCs does not alter SMC clonality in the carotid artery neointima following arterial ligation in young mice[40].

Although CHIP is detected by the presence of circulating leukocyte clones and is associated with an increased prevalence of cardiovascular disease, it has not been established whether leukocyte clones accumulate in the atherosclerotic plaque. Our results demonstrate patches of monocyte/macrophage clones in the plaques of aged mice (Fig. 1). Similarly, integrin β3 is reduced in monocytes/macrophages of aged mice and humans (Fig. 4), and *Itgb3*$^{(-/-)}$ monocytes/macrophages clonally expand in the atheroma (Fig. 5).

Among humans with CHIP and single *TET2* mutations, these mutations are, in most

cases, limited to the myeloid cell lineage[41]. CHIP with variant allele fractions as low as 10% or 1-2% have been associated with an elevated risk of atherosclerotic cardiovascular disease or heart failure, respectively[9,42]. As only a minority of leukocytes are affected, the increase in cardiovascular disease may be secondary to non-cell autonomous effects on vascular or cardiac cells[43]. Our studies demonstrate that *Tet2* null BM cells non-cell autonomously induce polyclonal expansion of SMCs in the plaque, and conditioned medium from *Tet2*$^{(-/-)}$ macrophages induces SMC migration and proliferation (Fig. 3).

Pivotal incompletely understood questions in regard to CHIP include in which downstream genes do mutations in epigenetic modulators induce expression changes and how do these mutations result in worsened atherosclerosis. TET2 catalyzes the conversion of 5mC to 5hmC, inducing gene expression, and a regulatory role for *Itgb3* promoter methylation has not been previously reported. Herein, we show that monocytes of aged mice and/or humans have reduced TET2 and integrin β3 levels and decreased levels of the 5hmC on the *ITGB3* promoter (Fig. 4). Similarly, in BM-derived monocytes of *Tet2*$^{(-/-)}$ mice, there are reduced levels of the Itgb3 transcript and of the 5hmC mark on the *Itgb3* promoter. Interestingly, the effects of aging on ITGB3 expression are cell type-specific as these levels are in fact increased in aged murine liver or human fibroblasts[44].

In humans, a polymorphism of the *ITGB3* gene (T1565C) is associated with coronary artery disease[45]. Mice with global *Itgb3* deletion or with *Itgb3* null BM have polyclonal SMC expansion in the atherosclerotic plaque and worse disease[2,20,46]. Herein, we find that deletion of *Itgb3* in monocytes/macrophages mimics results with *Itgb3*$^{(-/-)}$ BMT in terms of exacerbating atherosclerotic burden (Fig. 5). In contrast, SMC deletion of *Itgb3* attenuates atherosclerosis burden and SMC contribution to plaques but does not alter their clonality (Fig. S4). Interestingly,

the aged aorta has increased levels of the transmembrane protein CD47, which was initially co-purified with integrin β3 and regulates ligand binding of integrin αvβ3[ref. 47,48]. CD47 is implicated as a "don't eat me" signal, facilitating cellular evasion of efferocytosis in cancer and more recently in atherosclerosis as well, and CD47 marks SMA^+ cells, $CD68^+$ cells and caspase-3^+ cells in human carotid artery atheromas[49,50]. Treatment with an anti-CD47 antibody attenuates atherosclerosis and induces a more even distribution of colors of Rb-marked SMC-derived cells (i.e., polyclonal expansion)[26], but whether this finding is due to direct effects on SMCs and/or non-cell autonomous effects on other cells, such as immune cells, is not delineated. Future studies of cell-specific roles of CD47, its interplay with integrin β3 and downstream signaling in the context of atherosclerosis and aging are warranted.

The most significantly upregulated functional class of genes in *Tet2* null BM-derived macrophages consists of cytokines, chemokines and their receptors[9], and the CANTOS trial demonstrated benefit of the anti-IL1β drug canakinumab in patients with a previous myocardial infarction in select conditions[51]. Interestingly, an initial report of a subgroup analysis of CANTOS indicates that patients with *TET2* mutations and CHIP have an enhanced response to canakinumab[52]. Herein, scRNA-seq of *Itgb3* null BM-derived monocytes/macrophages demonstrate enhanced chemokine and cytokine signaling and in particular TNF signaling (Fig. 6). Plasma TNFα increases with aging, and studies suggest that the TNFα pathway positively regulates atherosclerosis and myocardial infarction[21,22,53]. Two SNPs of the *TNF receptor-1* (*TNFR1*) gene are associated with coronary artery disease in adults over 55 years old[54]. Furthermore, to evaluate underlying mechanisms, carotid arteries from aged and young $Tnfr1^{(-/-)}$ mice were grafted into $Apoe^{(-/-)}$ mice, and most interestingly, arteries from aged $Tnfr1^{(-/-)}$ mice are protected from age-induced atherosclerosis[54]. We now report that pharmacological inhibition of

TNFα attenuates atherosclerosis and limits the recruitment / clonal expansion of SMCs in *Itgb3*$^{(-/-)}$ or aged mice (Fig. 7). Additionally, rheumatoid arthritis is associated with increased atherosclerosis related cardiovascular disease, especially among the aged[55], and we suggest that some of the cardiovascular benefit of anti-TNFα drugs in this context[56,57] may result from limiting the clonal expansion of SMC progenitors.

Aging is the predominant risk factor for atherosclerosis and most chronic diseases in general. We demonstrate that aged macrophages express reduced levels of TET2 inhibiting Itgb3 expression. Decreased integrin β3 in macrophages enhances TNFα levels which induces polyclonal expansion of SMCs in the atherosclerotic plaque and worsens disease. Thus, our studies put forth deficient regulation of SMC clonal expansion by aged BM-derived macrophages as a critical underlying factor in the pathobiology of atherogenesis. Looking forward, this concept of impaired regulation of clonal expansion by aged BM (perhaps, via myeloid cell *Itgb3* deficiency) warrants intense investigation in other contexts, such as normal aging of the esophagus, endometrium, skin and bronchi as well as in cirrhosis and neurodegeneration[5,6,10-13].

Methods

Animals

Wild type (C57BL/6), *Ldlr*$^{(-/-)}$, *Apoe*$^{(-/-)}$, *Csf1r-Mer-iCre-Mer, ROSA26R*$^{(mTmG/mTmG)}$, *Itgb3*$^{(-/-)}$ and *Itgb3*$^{(flox/flox)}$ mice were purchased from The Jackson Laboratory[58-61]. Mice carrying *Myh11-CreER*^{T2} or the multi-color Rainbow (Rb) Cre reporter *ROSA26R*^{Rb} have been described[7,62,63]. Experiments with *Myh11-CreER*^{T2} mice are restricted to males as this transgene incorporated on the Y chromosome[63]. Otherwise, studies utilized adult both male and female mice. Three month (young) or 18 month old (aged) mice were used for most experiments.

Induction of atherogenesis and administration of AAV-*Pcsk9*

For atherosclerosis studies, we used mice null for *Ldlr*, *Apoe* and/or injected with recombinant adeno-associated virus (AAV) encoding constitutively active PCSK9 (*rAAV8.ApoEHCR-hAAT.D377Y-mPCSK9.bGH [*AAV-*Pcsk9]*); Penn Vector Core, University of Pennsylvania). For AAV-*Pcsk9* studies, one week after either tamoxifen treatment or, if relevant, four weeks after BMT, a single retro-orbital injection containing 1.0 x 10^{11} genome copies was administered. Four weeks later, mice were fed a WD (40% fat by calories, 1.25% cholesterol by weight; Research Diets Inc., D12108C) for up to 16 weeks. For mice not injected with AAV-*Pcsk9,* a WD was initiated four weeks after BMT.

Bone marrow transplantation

One week after tamoxifen treatment, mice that were to receive a BMT were first lethally irradiated with two doses of 550 rads (5.5 Gy) from a X-RAD 320 unit (Precision X-ray) administered 4 h apart. BM was collected from femurs and tibias of donor mice by flushing with

sterile Opti-MEM medium (Thermo Fisher). Each recipient mouse was injected retro-orbitally with 2×10^6 BM cells. Four weeks after BMT, peripheral blood was collected by retro-orbital venous plexus puncture, and genomic DNA was extracted with QIAamp DNA Blood Mini Kit (Qiagen, 51104) for PCR analysis of BM reconstitution. Primer sequences are provided in Table S2. Mice were then switched to a WD for up to 16 weeks and euthanized.

Tissue preparation, histology and morphometric analysis

Following euthanasia, the mouse heart with proximal ascending aorta attached was perfused with 10 ml of phosphate-buffered saline (PBS) through the left ventricle and then incubated in 4% paraformaldehyde (PFA) overnight at 4°C. The tissue was then washed with PBS and placed in 30% sucrose in PBS at 4°C until the next day. Finally, the heart with attached aorta was embedded in OCT (Tissue Tek), frozen, and stored at -80ºC. Serial cryosections of the aortic root were cut at 10 μm thickness using a cryostat. Every fifth pair of adjacent sections were stained with hematoxylin and eosin (H&E) and oil red O (ORO) for quantification of atherosclerotic plaque area and lipid deposition area, respectively. The size of the plaque and lipid areas for each mouse were obtained by averaging these areas from at least five sections. The necrotic core was measured as the average of acellular area of the plaque from three sections of the same mouse that were each at least 50 μm apart and reported as a percentage of the plaque area.

Immunohistochemistry

The aortic root was cryosectioned in the transverse axis, and 10 μm sections were incubated with blocking solution (0.1% Triton X-100 in PBS (PBS-T) supplemented with 5%

goat serum) and then with primary antibodies diluted in blocking solution overnight at 4°C. On the next day, sections were washed with PBS-T and then incubated with secondary antibodies for 1 h. Primary antibodies used were anti-GFP (1:500, Abcam, ab13970), anti-CD68 (1:200, Bio-Rad, MCA1957), directly conjugated Cy3 anti-SMA (1:500, Sigma-Aldrich, C6198). Secondary antibodies were conjugated to either FITC or Alexa-488, Alexa−647 fluorophores (1:500, Invitrogen). Nuclei were visualized by DAPI staining (1:1000, Sigma-Aldrich, D9542). Note, membrane-localized tdTomato (mT) fluorescence in the aorta of *ROSA26R*$^{(mTmG/+)}$ mice is very weak and essentially undetectable in comparison to the strong fluorescence in the red channel of staining with the anti-SMA antibody.

Fate mapping, clonal analysis and proliferation in atherogenesis

Mice carrying an inducible Cre recombinase and a Cre reporter [*ROSA26R*$^{(mTmG/+)}$ or *ROSA26R*$^{(Rb/+)}$] were induced with tamoxifen (1 mg/day) for 5 or 20 days in the case of *Myh11-CreER*^{T2} or *Csf1r-Mer-iCre-Mer*, respectively and then rested for one week. Following BMT and/or injection with AAV-*Pcsk9*, mice were fed a WD for up to 16 weeks and euthanized. For in vivo proliferation studies, 2.5 mg of 5-ethynyl-2' deoxyuridine (EdU) (Thermo Fisher Scientific, A10044) was injected intraperitoneally 12 h prior to euthanasia. Click-iT EdU Alexa Fluor 647 Imaging Kit (Thermo Fisher Scientific, C10340) was used as per manufacturer's instructions to detect EdU incorporation into proliferating cells. Serial sections through the aortic root were stained for nuclei (DAPI). In the case of mice carrying the *ROSA26R*$^{(mTmG/+)}$ reporter, sections were also stained for GFP and SMA and either EdU or CD68. For *ROSA26R*$^{(Rb/+)}$ mice, sections were directly imaged using fluorescent filters for Cerulean, mOrange, and mCherry, and marked cells in the media and plaque were quantified by scoring for expression of these

fluorophores. In all quantitative cellular studies, total cells were determined by counting $DAPI^+$ nuclei.

Anti-TNFα treatment

Mice underwent BMT, were rested for four weeks and then fed a WD for 12 weeks. During the WD feeding, mice were intraperitoneally injected twice per week with mouse monoclonal anti-TNFα antibody or IgG2a isotype matched control (Janssen Research and Development LLC, Spring House, PA) at a dose of 20 mg/kg body weight.

Isolation of mononuclear cells and monocytes from BM of mice

BM cells were harvested by flushing the femurs and tibias of mice in PBS with 2% fetal bovine serum (FBS) on ice. Mononuclear cells were isolated from BM cells by density gradient centrifugation using Lympholyte (Cedarlane, CL0531). After centrifugation at 1300 g for 20 min, mononuclear cells were collected from the interface and washed in Ca^{2+}/Mg^{2+} - free HBSS. The cells were dissociated to a single-cell suspension by filtering through a 70-μm nylon mesh. These mononuclear cells were subjected to scRNA-seq, monocyte isolation by FACS or differentiation to macrophages. For monocyte isolation, a suspension of mononuclear cells was stained with Alexa 700 anti-CD3 (1:100, BioLegend, 100215), PE-Cy7 anti-CD19 (1:100, BioLegend, 115520), FITC anti-CD11b (1:100, BD Pharmingen, 553310) and APC anti-Ly6c antibodies (1:100, BioLegend, 128015) in PBS with 0.5% FBS for 30 min. $CD11b^+Ly6c^+$ monocytes were isolated with a BD FACSAria II cell sorter.

Macrophage differentiation

Similar to our previous approach[2], BM-derived mononuclear cells were resuspended in Iscove's DMEM with 20% FBS, 20% L-929 cell conditioned medium, and 25 μg/ml fungizone and plated at a density of 1.8 x 10^6 cells/ml on uncoated plates. After 7 days of culture, non-adherent cells were washed away. Adherent cells were cultured in RPMI, 10% FBS for 12 h and then centrifuged at 1300 g for 5 min. The supernatant (i.e., macrophage conditioned medium) and pellet (i.e., macrophages) were used immediately or stored at -80°C.

Human peripheral blood monocyte isolation

Human peripheral blood mononuclear cells were isolated by Ficoll (GE Healthcare) density gradient centrifugation and then stained with PE anti-CD3 (1:100, BioLegend, 300308), PE-Cy7 anti-CD19 (1:100, BD Pharmingen, 115520) and FITC anti-CD14 (1:100, BioLegend, 325604). Human $CD14^+CD3^-CD19^-$ monocytes were sorted in a BD FACSAria II cell sorter.

Aortic SMC isolation

Aortic SMCs were isolated by modification of a previously described protocol[64]. Briefly, aortas from the root to the iliac bifurcation were harvested from adult wild type mice and opened longitudinally. Harvested aortas were enzymatically digested with 175 U/ml collagenase and 1.25 U/ml elastase (Worthington, LS004176 and LS002279, respectively) in PBS at 37°C in a shaking incubator for 30 min. The adventitia was manually peeled off, and the endothelium was removed by gentle scraping. Aortas were sequentially washed with 1% penicillin/streptomycin in PBS and then with 100% FBS. Washed aortas were cut into small pieces and cultured in plastic dishes in DMEM supplemented with 20% FBS, 1% penicillin/streptomycin. After 3 days, the medium was replaced by fresh medium that was the same except with 10% instead of 20% FBS.

SMCs that migrated out of the aortic pieces and adhered to the dish were trypsinized, expanded, and passaged. SMCs were used until the fifth passage.

Proliferation and migration assays in cell culture

For proliferation studies, wild type aortic SMC were cultured in DMEM, 10% FBS, 1% penicillin/streptomycin until they reached ~60% confluency. Cells were then serum starved in DMEM overnight, followed by incubation with macrophage-conditioned medium for 8 h or 48 h. During the last 8 h of this incubation, EdU (10 μM) from the Click-iT EdU Alexa Fluor 647 Imaging Kit (Thermo Fisher Scientific) was added to the conditioned medium. Subsequently, cells were fixed with 4% PFA for 30 min, permeabilized in 0.5% Triton X-100 in PBS and stained for EdU and nuclei (DAPI).

The migration assay used cell culture inserts (Ibidi), composed of two chambers flanking a central insert that prevents cell growth. Wild type aortic SMCs were added to both chambers and allowed to attach and grow to confluency. SMCs were serum starved overnight and washed with PBS prior to removal of the insert and then cultured in macrophage-conditioned medium for 6 h and 8 h. The cell coverage of the area that was blocked by the insert was measured immediately after insert removal and 6 h and 8 h later.

RNA isolation and quantitative real-time PCR

Total RNA was isolated from murine and human monocytes with the RNeasy Plus Micro Kit (Qiagen) and then 200 ng of RNA was reverse transcribed using the iScript RT Supermix (Bio-Rad), following instructions from the manufacturers. Quantitative real-time PCR was conducted in triplicate using SsoFast EvaGreen Supermix (Bio-Rad) on a Real Time Detection

System (Bio-Rad). Transcript levels are relative to that of Gapdh. Forward and reverse primers are listed in Table S3.

Western blot

Murine cells or aortic tissue were lysed in RIPA buffer containing complete protease inhibitor and phosphoSTOP phosphatase cocktails (Roche Applied Science). Lysate was centrifuged at 10,000 g for 10 min at 4°C, and the supernatant was collected. After estimating protein concentration with the BCA assay (Pierce), proteins were separated by SDS-PAGE and transferred overnight to nitrocellulose membranes (Millipore). Membranes were blocked with 5% bovine serum albumin in tris-buffered saline with 0.05% Tween-20 (TBS-T) for 1 h and incubated with primary antibody overnight at 4°C. Membranes were washed with TBS-T incubated with HRP-conjugated secondary antibodies (Dako). After washing in TBS-T again, protein detection was performed with Super Signal West Pico Chemiluminescent Substrate (Thermo Scientific) and GBOX Imaging System (Syngene). Primary antibodies used for Western blot analysis were anti-ITGB3 (1:1000, Abcam, ab197662), anti-phospho (S473) AKT (1:1000, Cell Signaling Technology, 4060), anti-total AKT (1:1000, Cell Signaling Technology, 4691), anti-phospho PAK1 (1:1000, Cell Signaling Technology, 2606), anti-total PAK1 (1:1000, Cell Signaling Technology, 2602), anti-phospho ERK (1:1000, Cell Signaling Technology, 4376), anti-total ERK (1:1000, Cell Signaling Technology, 4695), anti-TET2 (1:1000, Abcam, ab213369) and anti-GAPDH (1:1000, Cell Signaling Technology, 2118).

Hydroxymethyl DNA immunoprecipitation

Hydroxymethyl DNA immunoprecipitation (hMeDIP) was carried out using a hMeDIP kit (Diagenode, C02010031) as previously published[65]. Briefly, genomic DNA from murine or human monocytes was isolated using AllPrep DNA/RNA/miRNA Universal Kit (Qiagen, 80224). DNA (1 µg) was sheared with a sonicator, and DNA fragments (200 - 500 bp) were immunoprecipitated with a mouse monoclonal anti-5hmC antibody (2.5 µg per immunoprecipitation) following the protocol from Diagenode. The DNA-antibody mixture was incubated with magnetic beads overnight at 4°C, and then DNA was isolated. Multiple primers were designed to scan the proximal promoter region of *ITGB3* in murine and human monocytes. Open chromatin regions were identified using the UCSC genome browser (https://genome.ucsc.edu/). The forward and reverse primer pair spanning the proximal promoter region upstream of the transcription start site of mouse *Itgb3* were 5'-AGGATGCGAGCGCAGTG -3' and 5'- CGCACCTCTGCTTCTCAGT -3', respectively. The corresponding PCR amplification product is located at chr11:104,608,100 - 104,608,250. For human *ITGB3*, the forward and reverse primer pair spanning the promoter region upstream of the transcription start site were 5'- GAAGTGGTCAGGACCTGGAA-3' and 5'-TTCTGTGCCACTAGCCTGAG-3'. The location of this PCR amplification product is chr17:47,240,300 - 47,240,400. Hydroxymethylated DNA and input fractions were analyzed with hMeDIP-qPCR using *ITGB3* primers per the manufacturer's protocol to confirm enrichment of the hydroxymethylated gene.

Construction of 10X Genomics single cell 3' RNA-seq libraries and sequencing:

a) Gel Beads-In-Emulsion generation and barcoding

Single cell suspension of BM-derived mononuclear cells in RT Master Mix (75 μl) was loaded on the Single Cell A Chip and partitioned with a pool of ~750,000 barcoded gel beads to form nanoliter-scale Gel Beads-In-Emulsions (GEMs). Each gel bead has primers containing: (i) an Illumina R1 sequence (read 1 sequencing primer), (ii) a 16 nt 10x Barcode, (iii) a 10 nt Unique Molecular Identifier (UMI), and (iv) a poly-dT primer sequence. Upon dissolution of the Gel Beads in a GEM, the primers were released and mixed and incubated with cell lysate and RT Master Mix, producing barcoded, full-length cDNA from poly-adenylated mRNA.

b) Post GEM reverse transcription cleanup, cDNA amplification and library construction

Silane magnetic beads were used to isolate cDNA from leftover biochemical reagents and primers in the post GEM reaction mixture. Full-length, barcoded cDNA was then amplified by PCR to generate sufficient DNA for library construction. Enzymatic fragmentation and size selection were used to optimize cDNA amplicon size prior to library construction. R1 (read 1 primer sequence) were added during GEM incubation. P5, P7, a sample index, and R2 (read 2 primer sequence) were added during library construction via end repair, A-tailing, adaptor ligation and PCR. The final libraries contain the P5 and P7 primers used in Illumina bridge amplification.

c) Sequencing libraries

The single cell 3’ library comprised standard Illumina paired-end constructs which begin and end with P5 and P7. The single cell 3’ 16 bp 10x Barcode and 10 bp UMI were encoded in Read 1 and Read 2 was used for sequencing the cDNA fragment. Sequencing the single cell 3’

library produced standard Illumina Binary Base Call data which includes the paired-end Read 1 and Read 2 and the sample index in the i7 index read..

d) scRNA-seq data processing and analysis

Cellranger v3.1.0 was used to align scRNA-seq samples to the mouse genome (mm10). Downstream analysis was performed using Seurat v3.1.5 R package, including cell type identification and comparative analyses between the *Apoe*$^{(-/-)}$, *Itgb3*$^{(-/-)}$ and *Apoe*$^{(-/-)}$, *Itgb3*$^{(+/+)}$ samples. For quality control, cells with the number of expressed genes <100 or >6000 were filtered out. Cells were also excluded if their mitochondrial gene percentages were over 50%. For each sample, we first normalized the raw count matrix and then defined 2000 top variable genes. Seurat Integration was leveraged to find common anchoring features between these two samples and integrate them with default settings. We then applied principal component analysis for dimensionality reduction and retained 30 leading principal components for further visualization and cell clustering. The t-distributed stochastic neighbor embedding (t-SNE) projection[66] was used to visualize the cells on a two-dimensional space with a perplexity of 100. Subsequently, the share nearest neighbor graph was constructed by calculating the Jaccard index between each cell and its 20-nearest neighbors, which was then used for cell clustering based on Louvain algorithm (with a resolution of 0.125). After identifying cluster-specific genes, we annotated cell types based on some canonical marker genes. We removed erythroblasts and screened each cell type for differentially expressed genes between the two conditions. The gene lists served as the input to KEGG gene set enrichment analysis by using clusterProfiler v3.14.3 R package. IPA (Version 52912811, Ingenuity Systems, QIAGEN) was used to delineate diseases and functions represented by differentially expressed genes.

Bulk RNA sequencing:

a) RNA isolation and quality control

Total RNA from FACS-isolated monocytes was obtained using PureLink™ RNA Minikit (Invitrogen). RNA quality was determined by measuring A260/A280 and A260/A230 ratios via nanodrop. RNA integrity was determined by running an Agilent Bioanalyzer gel to measure the ratio of ribosomal peaks. Samples used for library preparation had RIN values greater than 8.

b) Bulk RNA-seq library preparation

mRNA was purified from ~200 ng of total RNA with oligo-dT beads and sheared by incubation at 94°C in the presence of Mg^{2+} with the KAPA mRNA HyperPrep kit (Roche). Following first-strand synthesis with random primers, second strand synthesis and A-tailing were performed with dUTP to generate strand-specific sequencing libraries. Adapter ligation with 3' dTMP overhangs were ligated to library insert fragments. Library amplification of fragments carrying the appropriate adapter sequences at both ends was undertaken. Strands marked with dUTP were not amplified. Indexed libraries were quantified by qRT-PCR using a commercially available kit (Roche, KAPA Biosystems) and insert size distribution was determined with the Agilent Bioanalyzer. Samples with a yield of ≥ 0.5 ng/µl and a size distribution of 150-300 bp were used for sequencing.

c) Flow cell preparation and sequencing

Samples at a concentration of 1.2 nM were loaded onto an Illumina NovaSeq6000 flow cell to yield 25 million passing filter clusters per sample. Samples were sequenced using 100 bp

paired-end sequencing per Illumina protocols. Reads were trimmed to remove low quality base calls.

d) Bulk RNA-seq analysis

STAR v2.5.3 was used to align the raw sequencing reads to the mouse genome (mm10) with default parameters. The number of reads for each gene was then counted with HTSeq v0.6.1. Subsequently, we used DESeq2 v1.26.0 R package to identify significantly differential expressed genes between aged and young BM-derived monocytes and then performed KEGG gene set enrichment analysis (GSEA) with clusterProfiler v3.14.3 R package.

Imaging

Images were acquired with Nikon microscopes (Eclipse 80i upright fluorescent or Eclipse TS100 inverted) or Leica SP8 confocal microscope. For image processing, analysis, and cell counting, Adobe Photoshop and Image J software were used.

Statistics

Two-tailed Student t-test and one-way ANOVA with Tukey's multiple comparison test were used to analyze data (GraphPad Prism 8). Data are presented as average ± SD. A p-value of ≤ 0.05 was considered statistically significant.

Study Approval

All mouse experiments were approved by the IACUC at Yale University and performed in accordance with relevant ethical guidelines. All procedures involving human subjects were

approved by the Institutional Review Boards of Yale University (IRB# 1005006865), and we complied with all relevant ethical regulations. Written informed consent was obtained from all participants prior to inclusion in the study.

Acknowledgements

We thank Greif laboratory members and Jeff Testani for input. I.K. was supported by a Postdoctoral Fellowship from the American Heart Association (18POST34030015). Funding was also provided by the NIH (R35HL150766, R01HL125815, R01HL142674, R21AG062202, 1R21NS123469 to D.M.G.), American Heart Association (Established Investigator Award, 19EIA34660321 to D.M.G.). No conflicts of interest.

Author contributions

I.K., J.D., R.C., R.Q., N.R., K.A.M., C.F.H., and D.M.G. conceived of and designed experiments. I.K., X.Z., J.D., R.C., R.R.C., A.N., B.A. and N.R. performed them. R.Q. and Y.K. conducted scRNA-seq analysis, and R.G-M. helped with bulk RNA-seq analysis. J.H. provided infrastructure for access to human blood. I.K. and D.M.G. analyzed the results, prepared the figures and wrote the manuscript. All authors reviewed and provided input on the manuscript.

Declaration of interests

The authors declare no competing interests.

Figure Legends

Figure 1. Age of mice dictates clonality of SMC- and macrophage-derived atherosclerotic plaque cells. Young (3 month) and aged (18 month) *ROSA26R*$^{(Rb/+)}$ mice also carrying either *Myh11-CreER*^{T2} or *Csf1r-Mer-iCre-Mer* were induced with tamoxifen, rested, injected with AAV-*Pcsk9* and fed a Western diet (WD) for 16 weeks. Transverse aortic root sections were analyzed. **a,** Schematic of experimental plan is shown. **b-e,** For *Myh11-CreER*^{T2}, *ROSA26R*$^{(Rb/+)}$ mice, sections were stained with H&E **(b;** dashed lines demarcating plaque**)**, or with Oil Red O **(**ORO; **c)**, and the area of the plaque **(d)** or lipid **(e)** were quantified, respectively. n=5-7 mice per group, triplicate measurements for each mouse. **f-l,** Sections were stained for nuclei (DAPI) and directly imaged for Rb colors (mCherry [mCh], mOrange [mOr], Cerulean [Cer]), and labeled cells were quantified. In **f, j,** representative sections are shown with boxed regions displayed as close-ups below. The percent of DAPI^{+} plaque cells that were marked by any of the Rb colors was quantified in **g, k**. In **h, l**, of the marked plaque cells, the percent of cells of each color was quantified for each age group. In a given plaque, color 1 is color with the greatest number of cells in plaque (or media), color 2 is second most common color and color 3 is least frequent color. n=5-7 mice and 18 plaques per age group, 5 sections with a total of ~1200-1600 cells and spanning 200 μm per plaque. Similarly, in **i**, of the marked cells of the underlying media, the precent of cells of each color was quantified. n=5 mice and 12 plaques analyzed per each group. Lu, lumen; Med, media; Pl, plaque. All data are mean ± SD, and Student's *t*-test was used. Scale bars, 100 μm (**b, c**) and 50 μm **(f, j)**.

Figure 2. Aged bone marrow promotes expansion of multiple SMMHC^{+} progenitors in the plaque. a-f, Young (3 month) *Ldlr*$^{(-/-)}$, *Myh11-CreER*^{T2}, *ROSA26R*$^{(Rb/+)}$ mice were induced with

tamoxifen, irradiated and then transplanted with bone marrow (BM) from young or aged (18 month) mice and fed a Western diet (WD) for 16 weeks. In **a,** experimental schematic is shown. In **b,** genomic DNA prepared from peripheral blood of *Ldlr*$^{(-/-)}$, *Myh11-CreER*^{T2}, *ROSA26R*$^{(Rb/+)}$ recipient mice following BMT from either young or aged wild type (WT) mice was PCR amplified using primers for *Ldlr*. Lanes 1-3 are from recipients with young BMT, and lanes 4-6 are from recipients with aged BMT. Lane 7 is from WT mice and lane 8 is from *Ldlr*$^{(-/-)}$ mice. In **c,** transverse aortic root sections were stained for nuclei (DAPI) and directly imaged for Rb colors (mCh, mOr, Cer) with boxed regions shown as close-ups below. In **d,** percent of DAPI^{+} plaque cells that were marked by any of the Rb colors was quantified. Of the marked plaque **(e)** or underlying medial cells **(f)**, percent of cells of each color was quantified for each BMT group. In a given plaque (or media), color 1 is color with the greatest number of cells, color 2 is second most common color and color 3 is least frequent color. n=5 mice and 15 plaques per BMT group, 5 sections with a total of ~1000-1500 cells and spanning 200 μm per plaque. Lu, lumen; Med, media; Pl, plaque. **g-j,** BM of young and aged wild type mice was harvested and differentiated into macrophages. Macrophage-conditioned medium (CM) was added to murine aortic SMCs for migration and proliferation assays. In **g, h,** for migration assay, confluent SMCs with a central acellular area were cultured in CM for 0, 6, or 8 h as indicated. Brightfield images **(g)** and quantification of the percent **(h)** of SMC coverage at 6 or 8 h of uncovered area of 0 h are shown, respectively. n=3. In **i, j,** for proliferation assay, SMCs were incubated with CM for 48 h, and EdU was added for last 8 h. SMCs were stained for EdU and nuclei **(**DAPI; **i)**, and percent of cells expressing EdU was quantified **(j)**. n=3 mice. All data are averages ± SD, and Student's *t*-test was used. Scale bars, 50 μm **(c, g)** and 25 μm **(i)**.

Figure 3. *Tet2* null BM induces expansion of multiple SMC progenitors in the plaque. a-f, Young (3 month) *Ldlr*$^{(-/-)}$, *Myh11-CreER*^{T2}, *ROSA26R*$^{(Rb/+)}$ mice were induced with tamoxifen, irradiated and then transplanted with BM from wild type (WT) or *Tet2*$^{(-/-)}$ mice and fed a WD for 16 weeks. In **a**, experimental schematic is shown. **b**, Genomic DNA prepared from peripheral blood of *Ldlr*$^{(-/-)}$, *Myh11-CreER*^{T2}, *ROSA26R*$^{(Rb/+)}$ recipient mice after either WT or *Tet2*$^{(-/-)}$ BM was PCR amplified using primers for *Tet2*. Lanes 1-3 are from recipient mice after WT BMT, lanes 4-6 are from recipient mice after *Tet2*$^{(-/-)}$ BMT, lane 7 is from WT mice and lane 8 is from *Tet2*$^{(-/-)}$ mice. In **c,** transverse aortic root sections were stained with DAPI and imaged for Rb colors. Boxed regions are shown as close-ups below. In **d,** percent of DAPI^{+} plaque cells that were marked by any Rb color was quantified. Of the marked plaque **(e)** or underlying medial cells **(f)**, percent of cells of each color was quantified for each BMT group. In a given plaque (or media), color 1 is color with greatest number of cells, color 2 is second most common color and color 3 is least frequent color. n=5 mice and 12 plaques per group, 5 sections with a total of ~1000-1500 cells and spanning 200 μm per plaque. Lu, lumen; Med, media; Pl, plaque. **g-j,** BM from *Tet2*$^{(-/-)}$ and wild type mice was harvested and differentiated into macrophages. Macrophage-CM was added to murine aortic SMCs for migration and proliferation assays. In **g, h,** for migration assay, confluent SMCs with a central area lacking cells were cultured in CM medium for 0, 6, or 8 h as indicated. Brightfield images **(g)** and quantification of percent **(h)** of SMC coverage at 6 or 8 h of uncovered area of 0 h are shown, respectively. n=3 mice. In **i, j,** for proliferation assay, murine aortic SMCs were incubated with CM for 48 h, and EdU was added for last 8 h. SMCs were stained for EdU and nuclei (DAPI; **i**), and percent of cells expressing EdU was quantified **(j)**. n=3. All data are averages ± SD, and Student's *t*-test was used. Scale bars, 50 μm **(c, g)** and 25 μm **(i)**.

Figure 4. Reduced TET2 contributes to decreased integrin β3 in aged myeloid cells. **a, b, d-i, k, l,** BM of young (3 month) and aged (18 month) mice **(a, b, d-i)** or young wild type or *Tet2*$^{(-/-)}$ mice **(k, l)** was harvested and either subjected to FACS to isolate $CD3^{-}CD19^{-}Cd11b^{+}Ly6C^{+}$ monocytes or differentiated into macrophages. **c, j,** Peripheral blood mononuclear cells were isolated from healthy young (25±3 yr) or older (55±7 yr) humans by Ficoll density gradient centrifugation. $CD3^{-}CD19^{-}CD14^{+}$ monocytes were isolated by FACS. In **a, b,** lysates of monocytes isolated from young or aged mice underwent bulk RNA-seq (n=3 mice per age group), and the transcriptome was subjected to pathway analysis. GSEA **(a)** shows activated pathways with gene ratio indicating the number of activated genes relative to the total number of genes in the corresponding pathways and size of the dot representing number of activated genes. Twenty differentially expressed genes (e.g., ITGB3 with green circle) significantly overlap with atherosclerosis in the Ingenuity Knowledge Base (**b**; $p = 7.52 \times 10^{-23}$). In **c, d,** qRT-PCR was used to measure ITGB3 RNA levels in lysates of human and murine monocytes, respectively. In **e, f,** after 7 days in culture to induce macrophage differentiation, the lysate of adherent murine cells was subjected to Western blot for integrin β3 and myeloid cell marker CSF1R. Densitometry of these proteins relative to GAPDH and normalized to cells isolated from young mice is shown. ns, not significant. In **g, h,** lysates of monocytes of young and aged mice were subjected to Western blot for TET2 and GAPDH with densitometry of TET2 relative to GAPDH. In **i-k,** hydroxymethyl DNA immunoprecipitation was performed with antibodies directed against 5hmC or IgG control. qRT-PCR was then conducted with primers specific for a region (chr11:104,608,100-104,608,250 in mice; chr17:47,240,300-47,240,400 in human) upstream of the *ITGB3* transcription start site. **p*<0.0001 vs. 5hmC, young (**i, j**) and wild type (**k**). In **l**, Itgb3

mRNA levels were measured in monocytes from wild type or *Tet2*$^{(-/-)}$ mice. n=12 humans and n=3-5 mice per age or genotype group. Data are mean ± SD. Student's *t*-test **(c, d, f, h, l)** and multifactor ANOVA with Tukey's post hoc test (**i-k**) were used.

Figure 5. Monocytes/macrophages deficient in *Itgb3* worsen atherosclerosis and clonally expand in the plaque. *Apoe*$^{(-/-)}$, *Csf1r-Mer-iCre-Mer* mice also carrying *Itgb3*$^{(flox/flox)}$ or wild type for *Itgb3* were induced with tamoxifen, rested, fed a WD and then transverse aortic root sections were analyzed. **a-d,** After 16 weeks of WD, sections were stained with H&E **(**dashed lines demarcate lesion; **a)** and Oil Red O **(b)** with quantification of lesion area **(c)** and lipid content **(d)**, respectively. n=5 mice per genotype, triplicate measurements per mouse. **e, f,** After 16 weeks of WD feeding to mice also carrying *ROSA26R*$^{(mTmG/+)}$, EdU was injected intraperitoneally 12 h prior to euthanasia. Sections were stained for markers of fate (GFP), SMCs (α-smooth muscle actin [SMA]), proliferation (EdU) and nuclei (DAPI) **(e)**. Boxed regions are shown as close-ups below with arrowheads indicating GFP$^+$EdU$^+$ cells. In **f,** the percentage of GFP$^+$ plaque cells that are EdU$^+$ is shown. n=5-7 mice and 10 plaques per genotype, 4 sections with a total of ~1000-1250 cells and spanning 150 μm per plaque. **g-i,** The duration of WD feeding in mice also carrying *ROSA26R*$^{(Rb/+)}$ was 6 or 9 weeks (w). Sections were stained with DAPI and directly imaged for Rb colors (mCh, mOr, Cer) with boxed regions shown as close-ups below (9 weeks WD in **g**). In **h,** the percent of DAPI$^+$ plaque cells that are also marked by any Rb color is shown. In **i,** of the marked plaque cells, the percent of cells of each color was quantified per age and genotype group. In a given plaque, color 1 is the color with greatest number of cells, color 2 is second most common and color 3 is least frequent. n=5-7 mice and 14 plaques per group, 5 sections with a total of ~1200-1400 cells and spanning 200 μm per plaque.

All data are averages ± SD, and Student's *t*-test was used. Scale bars, 100 μm **(a, b)** and 50 μm **(e, g)**.

Figure 6. *Itgb3*$^{(-/-)}$ monocytes/macrophages induce inflammatory pathways. scRNA-seq was conducted on BM cells isolated from *Apoe*$^{(-/-)}$ mice that are also either wild type or null for *Itgb3*. **a,** Overlayed t-SNE plots of scRNA-seq of BM cells from mice carrying *Itgb3*$^{(+/+)}$ (blue) or *Itgb3*$^{(-/-)}$ (red) are shown. **b**, t-SNE plot combining cells of both genotypes with distinct clusters that are identified as major cell types based on expression levels of cluster markers (see Fig. S6). **c-e,** Pathway and gene expression analysis of single cell transcriptomes of the monocyte/macrophage cluster. In **c,** GSEA identifies activated pathways. Gene ratio indicates the number of activated genes relative to the total number of genes in the corresponding pathway, and dot size represents the number of dysregulated genes in each pathway. In **d,** dot plot analysis of differentially expressed genes in TNFα, chemokine, and cytokine signaling pathways. Dot size and red color represent the fraction of cells expressing the gene and the average gene expression, respectively. **e**, IPA predicts the effects of differentially expressed genes on the inflammatory responses and monocyte/macrophage migration or proliferation. n=3 mice pooled per genotype.

Figure 7. In the context of *Itgb3*$^{(-/-)}$ BM, TNFα antagonism preserves predominance of a single SMC clone in plaques. Mice were treated with 12 weeks of WD with concomitant two times per week injections of isotype control IgG2a or anti-TNFα antibody (20 mg/kg) and then transverse aortic root sections were analyzed. **a-e,** Prior to these treatments, *Apoe*$^{(-/-)}$, *Csf1r-Mer-iCre-Mer* mice also carrying *Itgb3*$^{(flox/flox)}$ or wild type for *Itgb3* were induced with tamoxifen and rested. In **a,** experimental schematic is shown. Sections were stained with H&E **(**dashed lines

demarcate lesion; **b)** and Oil Red O **(c)**, and lesion area **(d)** and lipid content **(e)** were quantified. **f-m**, Prior to the WD and treatment with control or anti-TNFα antibody, *Apoe*$^{(-/-)}$, *Myh11-CreER*^{T2}, *ROSA26R*$^{(Rb/+)}$ mice were induced with tamoxifen, irradiated and then transplanted with *Apoe*$^{(-/-)}$ BM also carrying *Itgb3*$^{(+/+)}$ or *Itgb3*$^{(-/-)}$ as indicated. In **f, g,** schematic is shown. In **h,** genomic DNA prepared from peripheral blood of *Apoe*$^{(-/-)}$, *Myh11-CreER*^{T2}, *ROSA26R*$^{(Rb/+)}$ recipient mice with *Apoe*$^{(-/-)}$, *Itgb3*$^{(+/+)}$ or *Apoe*$^{(-/-)}$, *Itgb3*$^{(-/-)}$ BM or of WT or *Itgb3*$^{(-/-)}$ mice was amplified using primers for *Itgb3*. In **i, j,** sections were stained with DAPI and directly imaged for Rb colors. In **k,** percent of DAPI^{+} plaque cells that were marked by any Rb color was quantified. Of the marked plaque **(l)** or underlying medial cells **(m)**, the percent of cells of each color was quantified for each BMT and treatment group. In a given plaque (or media), color 1 is the most dominant color of cells, color 2 is the second most prevalent and color 3 is least frequent. n=5 mice and 12 plaques per group, 5-6 sections with a total of ~1150-1650 cells and spanning 200 μm per plaque. All data are averages ± SD, and Student's *t*-test was used. Lu, lumen; Med, media; Pl, plaque. Scale bars, 200 μm **(b, c)** and 50 μm **(i, j)**.

References

1. Sheikh AQ, Misra A, Rosas IO, Adams RH, Greif DM. Smooth muscle cell progenitors are primed to muscularize in pulmonary hypertension. *Sci Transl Med.* 2015;7(308):308ra159.

2. Misra A, Feng Z, Chandran RR, Kabir I, Rotllan N, Aryal B, Sheikh AQ, Ding L, Qin L, Fernandez-Hernando C, Tellides G, Greif DM. Integrin beta3 regulates clonality and fate of smooth muscle-derived atherosclerotic plaque cells. *Nat Commun.* 2018;9(1):2073.

3. Chappell J, Harman JL, Narasimhan VM, Yu H, Foote K, Simons BD, Bennett MR, Jorgensen HF. Extensive Proliferation of a Subset of Differentiated, yet Plastic, Medial Vascular Smooth Muscle Cells Contributes to Neointimal Formation in Mouse Injury and Atherosclerosis Models. *Circ Res.* 2016;119(12):1313-1323.

4. Jacobsen K, Lund MB, Shim J, Gunnersen S, Fuchtbauer EM, Kjolby M, Carramolino L, Bentzon JF. Diverse cellular architecture of atherosclerotic plaque derives from clonal expansion of a few medial SMCs. *JCI Insight.* 2017;2(19).

5. Tay TL, Mai D, Dautzenberg J, Fernandez-Klett F, Lin G, Sagar, Datta M, Drougard A, Stempfl T, Ardura-Fabregat A, Staszewski O, Margineanu A, Sporbert A, Steinmetz LM, Pospisilik JA, Jung S, Priller J, Grun D, Ronneberger O, Prinz M. A new fate mapping system reveals context-dependent random or clonal expansion of microglia. *Nat Neurosci.* 2017;20(6):793-803.

6. Brunner SF, Roberts ND, Wylie LA, Moore L, Aitken SJ, Davies SE, Sanders MA, Ellis P, Alder C, Hooks Y, Abascal F, Stratton MR, Martincorena I, Hoare M, Campbell PJ. Somatic mutations and clonal dynamics in healthy and cirrhotic human liver. *Nature.* 2019;574(7779):538-542.

7. Greif DM, Kumar M, Lighthouse JK, Hum J, An A, Ding L, Red-Horse K, Espinoza FH, Olson L, Offermanns S, Krasnow MA. Radial construction of an arterial wall. *Dev Cell.* 2012;23(3):482-493.

8. Jaiswal S, Libby P. Clonal haematopoiesis: connecting ageing and inflammation in cardiovascular disease. *Nat Rev Cardiol.* 2020;17(3):137-144.

9. Jaiswal S, Natarajan P, Silver AJ, Gibson CJ, Bick AG, Shvartz E, McConkey M, Gupta N, Gabriel S, Ardissino D, Baber U, Mehran R, Fuster V, Danesh J, Frossard P, Saleheen D, Melander O, Sukhova GK, Neuberg D, Libby P, Kathiresan S, Ebert BL. Clonal Hematopoiesis and Risk of Atherosclerotic Cardiovascular Disease. *N Engl J Med.* 2017;377(2):111-121.

10. Martincorena I, Fowler JC, Wabik A, Lawson ARJ, Abascal F, Hall MWJ, Cagan A, Murai K, Mahbubani K, Stratton MR, Fitzgerald RC, Handford PA, Campbell PJ, Saeb-Parsy K, Jones PH. Somatic mutant clones colonize the human esophagus with age. *Science.* 2018;362(6417):911-917.

11. Moore L, Leongamornlert D, Coorens THH, Sanders MA, Ellis P, Dentro SC, Dawson KJ, Butler T, Rahbari R, Mitchell TJ, Maura F, Nangalia J, Tarpey PS, Brunner SF, Lee-Six H, Hooks Y, Moody S, Mahbubani KT, Jimenez-Linan M, Brosens JJ, Iacobuzio-Donahue CA, Martincorena I, Saeb-Parsy K, Campbell PJ, Stratton MR. The mutational landscape of normal human endometrial epithelium. *Nature.* 2020;580(7805):640-646.

12. Martincorena I, Roshan A, Gerstung M, Ellis P, Van Loo P, McLaren S, Wedge DC, Fullam A, Alexandrov LB, Tubio JM, Stebbings L, Menzies A, Widaa S, Stratton MR, Jones PH, Campbell PJ. Tumor evolution. High burden and pervasive positive selection of somatic mutations in normal human skin. *Science.* 2015;348(6237):880-886.

13. Yoshida K, Gowers KHC, Lee-Six H, Chandrasekharan DP, Coorens T, Maughan EF, Beal K, Menzies A, Millar FR, Anderson E, Clarke SE, Pennycuick A, Thakrar RM, Butler CR, Kakiuchi N, Hirano T, Hynds RE, Stratton MR, Martincorena I, Janes SM, Campbell PJ. Tobacco smoking and somatic mutations in human bronchial epithelium. *Nature.* 2020;578(7794):266-272.

14. Palmer S, Albergante L, Blackburn CC, Newman TJ. Reply to Jimenez-Alonso et al., Schooling and Zhao, and Mortazavi: Further discussion on the immunological model of carcinogenesis. *Proc Natl Acad Sci U S A.* 2018;115(19):E4319-E4321.

15. Palmer S, Albergante L, Blackburn CC, Newman TJ. Thymic involution and rising disease incidence with age. *Proc Natl Acad Sci U S A.* 2018;115(8):1883-1888.

16. Tyrrell DJ, Goldstein DR. Ageing and atherosclerosis: vascular intrinsic and extrinsic factors and potential role of IL-6. *Nat Rev Cardiol.* 2021;18(1):58-68.

17. Basatemur GL, Jorgensen HF, Clarke MCH, Bennett MR, Mallat Z. Vascular smooth muscle cells in atherosclerosis. *Nat Rev Cardiol.* 2019;16(12):727-744.

18. Shankman LS, Gomez D, Cherepanova OA, Salmon M, Alencar GF, Haskins RM, Swiatlowska P, Newman AA, Greene ES, Straub AC, Isakson B, Randolph GJ, Owens GK. KLF4-dependent phenotypic modulation of smooth muscle cells has a key role in atherosclerotic plaque pathogenesis. *Nat Med.* 2015;21(6):628-637.

19. Wirka RC, Wagh D, Paik DT, Pjanic M, Nguyen T, Miller CL, Kundu R, Nagao M, Coller J, Koyano TK, Fong R, Woo YJ, Liu B, Montgomery SB, Wu JC, Zhu K, Chang R, Alamprese M, Tallquist MD, Kim JB, Quertermous T. Atheroprotective roles of smooth muscle cell phenotypic modulation and the TCF21 disease gene as revealed by single-cell analysis. *Nat Med.* 2019;25(8):1280-1289.

20. Schneider JG, Zhu Y, Coleman T, Semenkovich CF. Macrophage beta3 integrin suppresses hyperlipidemia-induced inflammation by modulating TNFalpha expression. *Arterioscler Thromb Vasc Biol.* 2007;27(12):2699-2706.

21. Bruunsgaard H, Skinhoj P, Pedersen AN, Schroll M, Pedersen BK. Ageing, tumour necrosis factor-alpha (TNF-alpha) and atherosclerosis. *Clin Exp Immunol.* 2000;121(2):255-260.

22. Bauernfeind F, Niepmann S, Knolle PA, Hornung V. Aging-Associated TNF Production Primes Inflammasome Activation and NLRP3-Related Metabolic Disturbances. *J Immunol.* 2016;197(7):2900-2908.

23. Du W, Wong C, Song Y, Shen H, Mori D, Rotllan N, Price N, Dobrian AD, Meng H, Kleinstein SH, Fernandez-Hernando C, Goldstein DR. Age-associated vascular inflammation promotes monocytosis during atherogenesis. *Aging Cell.* 2016;15(4):766-777.

24. Fuster JJ, MacLauchlan S, Zuriaga MA, Polackal MN, Ostriker AC, Chakraborty R, Wu CL, Sano S, Muralidharan S, Rius C, Vuong J, Jacob S, Muralidhar V, Robertson AA, Cooper MA, Andres V, Hirschi KK, Martin KA, Walsh K. Clonal hematopoiesis associated with TET2 deficiency accelerates atherosclerosis development in mice. *Science.* 2017;355(6327):842-847.

25. Robbins CS, Hilgendorf I, Weber GF, Theurl I, Iwamoto Y, Figueiredo JL, Gorbatov R, Sukhova GK, Gerhardt LM, Smyth D, Zavitz CC, Shikatani EA, Parsons M, van Rooijen N, Lin HY, Husain M, Libby P, Nahrendorf M, Weissleder R, Swirski FK. Local proliferation dominates lesional macrophage accumulation in atherosclerosis. *Nat Med.* 2013;19(9):1166-1172.

26. Wang Y, Nanda V, Direnzo D, Ye J, Xiao S, Kojima Y, Howe KL, Jarr KU, Flores AM, Tsantilas P, Tsao N, Rao A, Newman AAC, Eberhard AV, Priest JR, Ruusalepp A, Pasterkamp G, Maegdefessel L, Miller CL, Lind L, Koplev S, Bjorkegren JLM, Owens GK, Ingelsson E, Weissman IL, Leeper NJ. Clonally expanding smooth muscle cells promote atherosclerosis by escaping efferocytosis and activating the complement cascade. *Proc Natl Acad Sci U S A.* 2020;117(27):15818-15826.

27. Ntokou A, Dave JM, Kauffman AC, Sauler M, Ryu C, Hwa J, Herzog EL, Singh I, Saltzman WM, Greif DM. Macrophage-derived PDGF-B induces muscularization in murine and human pulmonary hypertension. *JCI Insight.* 2021;6(6).

28. Nelson PR, Yamamura S, Mureebe L, Itoh H, Kent KC. Smooth muscle cell migration and proliferation are mediated by distinct phases of activation of the intracellular messenger mitogen-activated protein kinase. *J Vasc Surg.* 1998;27(1):117-125.

29. Stabile E, Zhou YF, Saji M, Castagna M, Shou M, Kinnaird TD, Baffour R, Ringel MD, Epstein SE, Fuchs S. Akt controls vascular smooth muscle cell proliferation in vitro and in vivo by delaying G1/S exit. *Circ Res.* 2003;93(11):1059-1065.

30. Gerthoffer WT. Mechanisms of vascular smooth muscle cell migration. *Circ Res.* 2007;100(5):607-621.

31. Fernández-Hernando C, József L, Jenkins D, Di Lorenzo A, Sessa WC. Absence of Akt1 reduces vascular smooth muscle cell migration and survival and induces features of plaque vulnerability and cardiac dysfunction during atherosclerosis. *Arterioscler Thromb Vasc Biol.* 2009;29(12):2033-2040.

32. Gu Z, Noss EH, Hsu VW, Brenner MB. Integrins traffic rapidly via circular dorsal ruffles and macropinocytosis during stimulated cell migration. *J Cell Biol.* 2011;193(1):61-70.

33. Branen L, Hovgaard L, Nitulescu M, Bengtsson E, Nilsson J, Jovinge S. Inhibition of tumor necrosis factor-alpha reduces atherosclerosis in apolipoprotein E knockout mice. *Arterioscler Thromb Vasc Biol.* 2004;24(11):2137-2142.

34. Oberoi R, Vlacil AK, Schuett J, Schosser F, Schuett H, Tietge UJF, Schieffer B, Grote K. Anti-tumor necrosis factor-alpha therapy increases plaque burden in a mouse model of experimental atherosclerosis. *Atherosclerosis.* 2018;277:80-89.

35. Lee-Six H, Olafsson S, Ellis P, Osborne RJ, Sanders MA, Moore L, Georgakopoulos N, Torrente F, Noorani A, Goddard M, Robinson P, Coorens THH, O'Neill L, Alder C, Wang J, Fitzgerald RC, Zilbauer M, Coleman N, Saeb-Parsy K, Martincorena I, Campbell PJ, Stratton MR. The landscape of somatic mutation in normal colorectal epithelial cells. *Nature.* 2019;574(7779):532-537.

36. Fearon ER, Vogelstein B. A genetic model for colorectal tumorigenesis. *Cell.* 1990;61(5):759-767.

37. Bjorklund MM, Hollensen AK, Hagensen MK, Dagnaes-Hansen F, Christoffersen C, Mikkelsen JG, Bentzon JF. Induction of atherosclerosis in mice and hamsters without germline genetic engineering. *Circ Res.* 2014;114(11):1684-1689.

38. Roche-Molina M, Sanz-Rosa D, Cruz FM, Garcia-Prieto J, Lopez S, Abia R, Muriana FJ, Fuster V, Ibanez B, Bernal JA. Induction of sustained hypercholesterolemia by single adeno-associated virus-mediated gene transfer of mutant hPCSK9. *Arterioscler Thromb Vasc Biol.* 2015;35(1):50-59.

39. Tyrrell DJ, Blin M, Song J, Wood S, Zhang M, Beard DA, Goldstein D. Age-Associated Mitochondrial Dysfunction Accelerates Atherogenesis. *Circ Res.* 2019.

40. Uryga AK, Grootaert MOJ, Garrido AM, Oc S, Foote K, Chappell J, Finigan A, Rossiello F, d'Adda di Fagagna F, Aravani D, Jorgensen HF, Bennett MR. Telomere damage promotes vascular smooth muscle cell senescence and immune cell recruitment after vessel injury. *Commun Biol.* 2021;4(1):611.

41. Buscarlet M, Provost S, Zada YF, Bourgoin V, Mollica L, Dubé MP, Busque L. Lineage restriction analyses in CHIP indicate myeloid bias for TET2 and multipotent stem cell origin for DNMT3A. *Blood.* 2018;132(3):277-280.

42. Dorsheimer L, Assmus B, Rasper T, Ortmann CA, Ecke A, Abou-El-Ardat K, Schmid T, Brune B, Wagner S, Serve H, Hoffmann J, Seeger F, Dimmeler S, Zeiher AM, Rieger MA. Association of Mutations Contributing to Clonal Hematopoiesis With Prognosis in Chronic Ischemic Heart Failure. *JAMA Cardiol.* 2019;4(1):25-33.

43. Cobo I, Tanaka T, Glass CK, Yeang C. Clonal hematopoiesis driven by DNMT3A and TET2 mutations: role in monocyte and macrophage biology and atherosclerotic cardiovascular disease. *Curr Opin Hematol.* 2021.

44. Rapisarda V, Borghesan M, Miguela V, Encheva V, Snijders AP, Lujambio A, O'Loghlen A. Integrin Beta 3 Regulates Cellular Senescence by Activating the TGF-beta Pathway. *Cell Rep.* 2017;18(10):2480-2493.

45. Bogatyreva KB, Azova MM, Aghajanyan AV, Tskhovrebova LV, Ait AA, Shugushev ZK. Association of the ITGB3 gene T1565C polymorphism with the development of atherosclerosis and in-stent restenosis in patients with stable coronary artery disease. *Research Results in Biomedicine.* 2018;4(4):3-9.

46. Weng S, Zemany L, Standley KN, Novack DV, La Regina M, Bernal-Mizrachi C, Coleman T, Semenkovich CF. Beta3 integrin deficiency promotes atherosclerosis and pulmonary

inflammation in high-fat-fed, hyperlipidemic mice. *Proc Natl Acad Sci U S A.* 2003;100(11):6730-6735.

47. Brown E, Hooper L, Ho T, Gresham H. Integrin-associated protein: a 50-kD plasma membrane antigen physically and functionally associated with integrins. *J Cell Biol.* 1990;111(6 Pt 1):2785-2794.

48. Lindberg FP, Gresham HD, Schwarz E, Brown EJ. Molecular cloning of integrin-associated protein: an immunoglobulin family member with multiple membrane-spanning domains implicated in alpha v beta 3-dependent ligand binding. *J Cell Biol.* 1993;123(2):485-496.

49. Kojima Y, Volkmer JP, McKenna K, Civelek M, Lusis AJ, Miller CL, Direnzo D, Nanda V, Ye J, Connolly AJ, Schadt EE, Quertermous T, Betancur P, Maegdefessel L, Matic LP, Hedin U, Weissman IL, Leeper NJ. CD47-blocking antibodies restore phagocytosis and prevent atherosclerosis. *Nature.* 2016;536(7614):86-90.

50. Chao MP, Majeti R, Weissman IL. Programmed cell removal: a new obstacle in the road to developing cancer. *Nature Reviews Cancer.* 2012;12(1):58-67.

51. Ridker PM, Everett BM, Thuren T, MacFadyen JG, Chang WH, Ballantyne C, Fonseca F, Nicolau J, Koenig W, Anker SD, Kastelein JJP, Cornel JH, Pais P, Pella D, Genest J, Cifkova R, Lorenzatti A, Forster T, Kobalava Z, Vida-Simiti L, Flather M, Shimokawa H, Ogawa H, Dellborg M, Rossi PRF, Troquay RPT, Libby P, Glynn RJ, Group CT. Antiinflammatory Therapy with Canakinumab for Atherosclerotic Disease. *N Engl J Med.* 2017;377(12):1119-1131.

52. Svensson EC, Madar A, Campbell CD, He Y, Sultan M, Healey ML, D'Aco K, Fernandez A, Wache-Mainier C, Ridker PM, Beste MT, Basson CT. Abstract 15111: TET2-Driven

Clonal Hematopoiesis Predicts Enhanced Response to Canakinumab in the CANTOS Trial: An Exploratory Analysis. *Circulation.* 2018;138:A15111.

53. Ridker PM, Rifai N, Pfeffer M, Sacks F, Lepage S, Braunwald E. Elevation of tumor necrosis factor-alpha and increased risk of recurrent coronary events after myocardial infarction. *Circulation.* 2000;101(18):2149-2153.

54. Zhang L, Connelly JJ, Peppel K, Brian L, Shah SH, Nelson S, Crosslin DR, Wang T, Allen A, Kraus WE, Gregory SG, Hauser ER, Freedman NJ. Aging-related atherosclerosis is exacerbated by arterial expression of tumor necrosis factor receptor-1: evidence from mouse models and human association studies. *Hum Mol Genet.* 2010;19(14):2754-2766.

55. Crowson CS, Therneau TM, Davis JM, 3rd, Roger VL, Matteson EL, Gabriel SE. Brief report: accelerated aging influences cardiovascular disease risk in rheumatoid arthritis. *Arthritis and rheumatism.* 2013;65(10):2562-2566.

56. Dixon WG, Watson KD, Lunt M, Hyrich KL, British Society for Rheumatology Biologics Register Control Centre C, Silman AJ, Symmons DP, British Society for Rheumatology Biologics R. Reduction in the incidence of myocardial infarction in patients with rheumatoid arthritis who respond to anti-tumor necrosis factor alpha therapy: results from the British Society for Rheumatology Biologics Register. *Arthritis Rheum.* 2007;56(9):2905-2912.

57. Westlake SL, Colebatch AN, Baird J, Curzen N, Kiely P, Quinn M, Choy E, Ostor AJ, Edwards CJ. Tumour necrosis factor antagonists and the risk of cardiovascular disease in patients with rheumatoid arthritis: a systematic literature review. *Rheumatology (Oxford).* 2011;50(3):518-531.

58. Qian BZ, Li J, Zhang H, Kitamura T, Zhang J, Campion LR, Kaiser EA, Snyder LA, Pollard JW. CCL2 recruits inflammatory monocytes to facilitate breast-tumour metastasis. *Nature.* 2011;475(7355):222-225.

59. Muzumdar MD, Tasic B, Miyamichi K, Li L, Luo L. A global double-fluorescent Cre reporter mouse. *Genesis.* 2007;45(9):593-605.

60. Hodivala-Dilke KM, McHugh KP, Tsakiris DA, Rayburn H, Crowley D, Ullman-Cullere M, Ross FP, Coller BS, Teitelbaum S, Hynes RO. Beta3-integrin-deficient mice are a model for Glanzmann thrombasthenia showing placental defects and reduced survival. *J Clin Invest.* 1999;103(2):229-238.

61. Morgan EA, Schneider JG, Baroni TE, Uluckan O, Heller E, Hurchla MA, Deng H, Floyd D, Berdy A, Prior JL, Piwnica-Worms D, Teitelbaum SL, Ross FP, Weilbaecher KN. Dissection of platelet and myeloid cell defects by conditional targeting of the beta3-integrin subunit. *FASEB J.* 2010;24(4):1117-1127.

62. Rinkevich Y, Lindau P, Ueno H, Longaker MT, Weissman IL. Germ-layer and lineage-restricted stem/progenitors regenerate the mouse digit tip. *Nature.* 2011;476(7361):409-413.

63. Wirth A, Benyo Z, Lukasova M, Leutgeb B, Wettschureck N, Gorbey S, Orsy P, Horvath B, Maser-Gluth C, Greiner E, Lemmer B, Schutz G, Gutkind JS, Offermanns S. G12-G13-LARG-mediated signaling in vascular smooth muscle is required for salt-induced hypertension. *Nat Med.* 2008;14(1):64-68.

64. Karnik SK, Brooke BS, Bayes-Genis A, Sorensen L, Wythe JD, Schwartz RS, Keating MT, Li DY. A critical role for elastin signaling in vascular morphogenesis and disease. *Development.* 2003;130(2):411-423.

65. Liu R, Jin Y, Tang WH, Qin L, Zhang X, Tellides G, Hwa J, Yu J, Martin KA. Ten-eleven translocation-2 (TET2) is a master regulator of smooth muscle cell plasticity. *Circulation.* 2013;128(18):2047-2057.

66. Linderman GC, Rachh M, Hoskins JG, Steinerberger S, Kluger Y. Fast interpolation-based t-SNE for improved visualization of single-cell RNA-seq data. *Nat Methods.* 2019;16(3):243-245.

AAV-*Pcsk9*, WD 16 Weeks

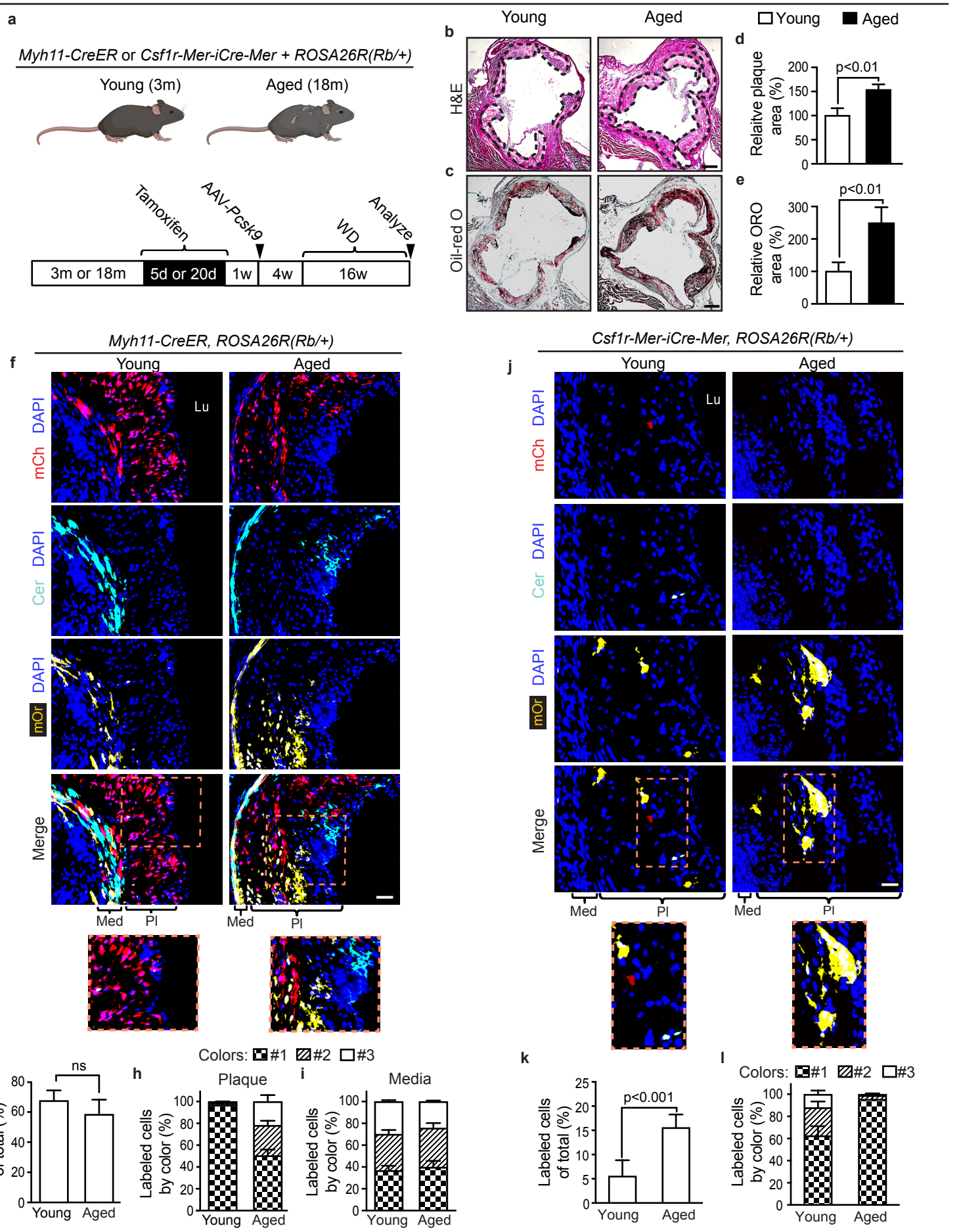

Young *Ldlr(-/-), Myh11-CreER, ROSA26R(Rb/+)*, BMT (Young vs Aged), WD 16 Weeks

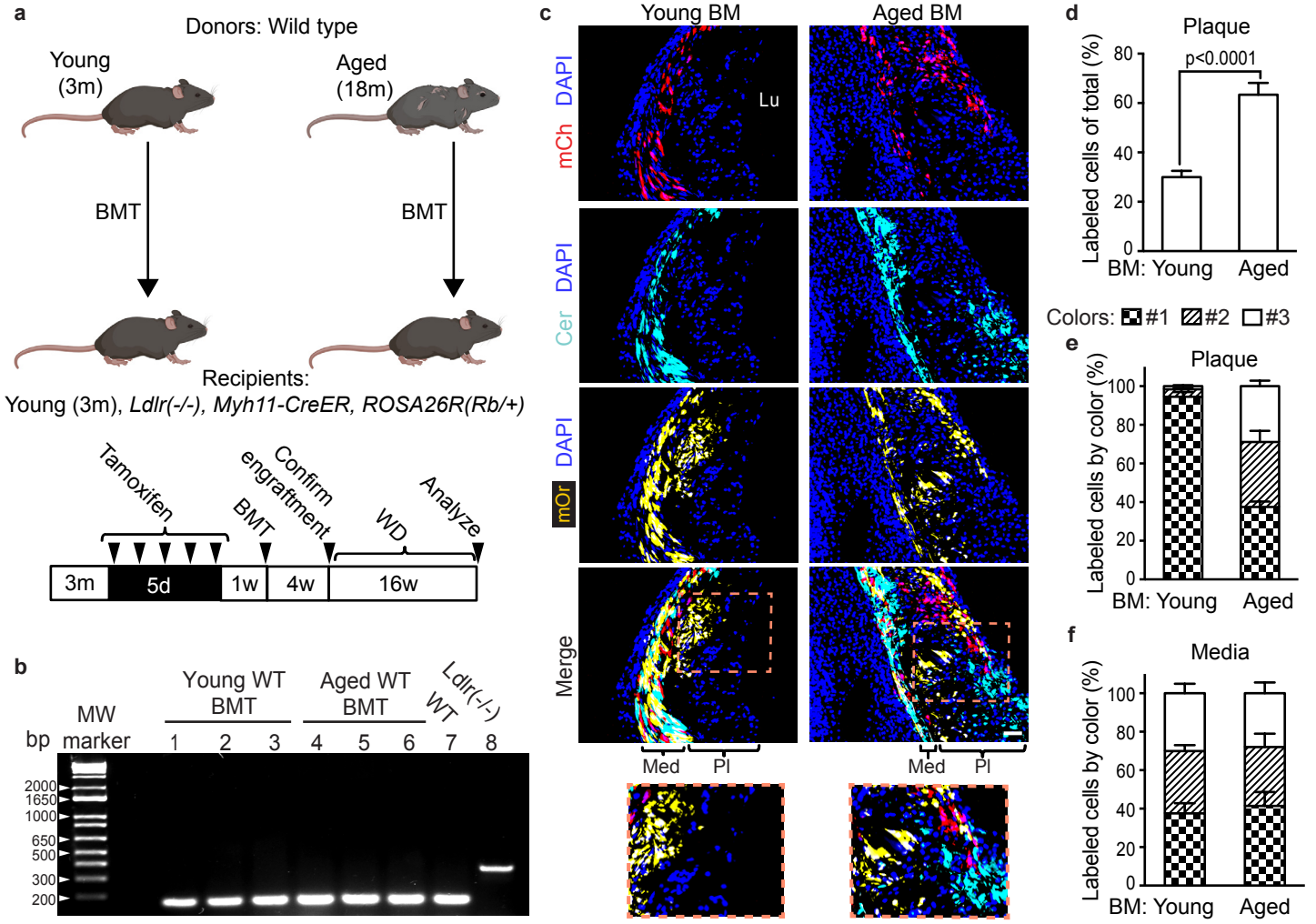

SMC culture in Mø-conditioned medium

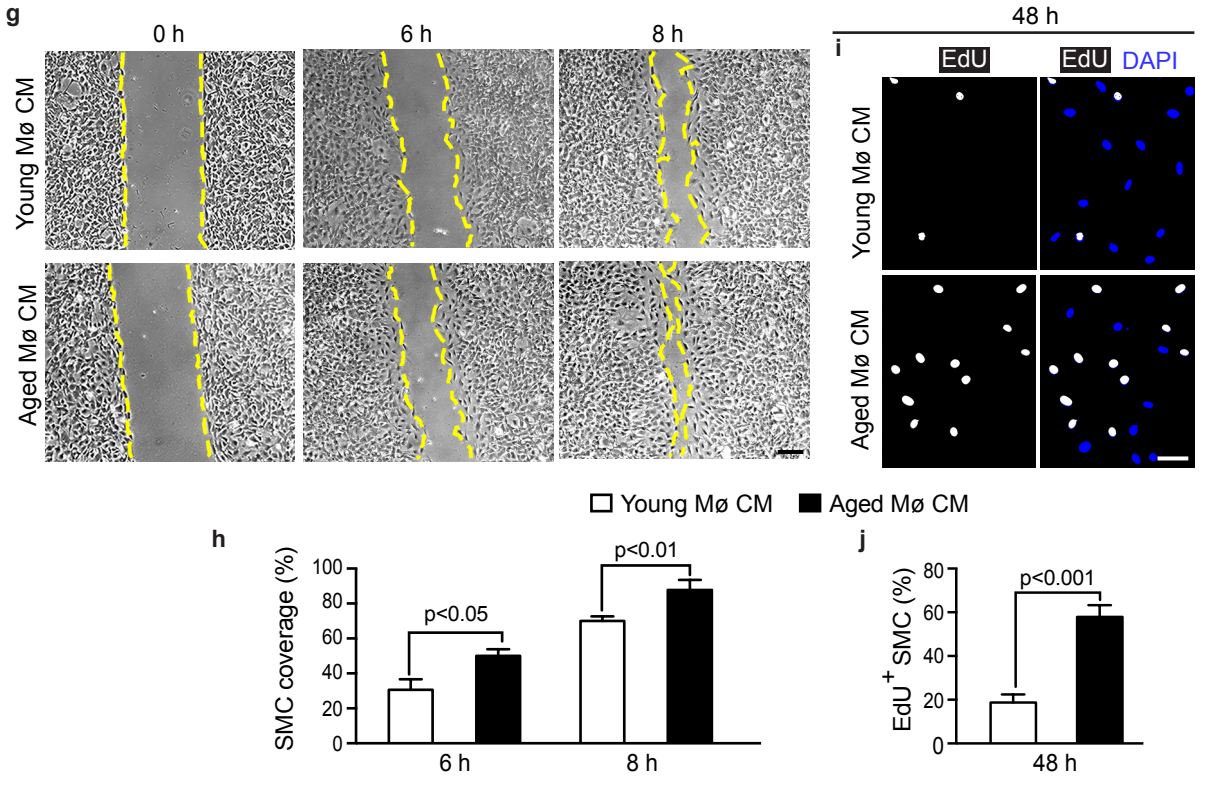

Young *Ldlr(-/-), Myh11-CreER, ROSA26R(Rb/+),* BMT [WT vs *Tet2(-/-)*], WD 16 Weeks

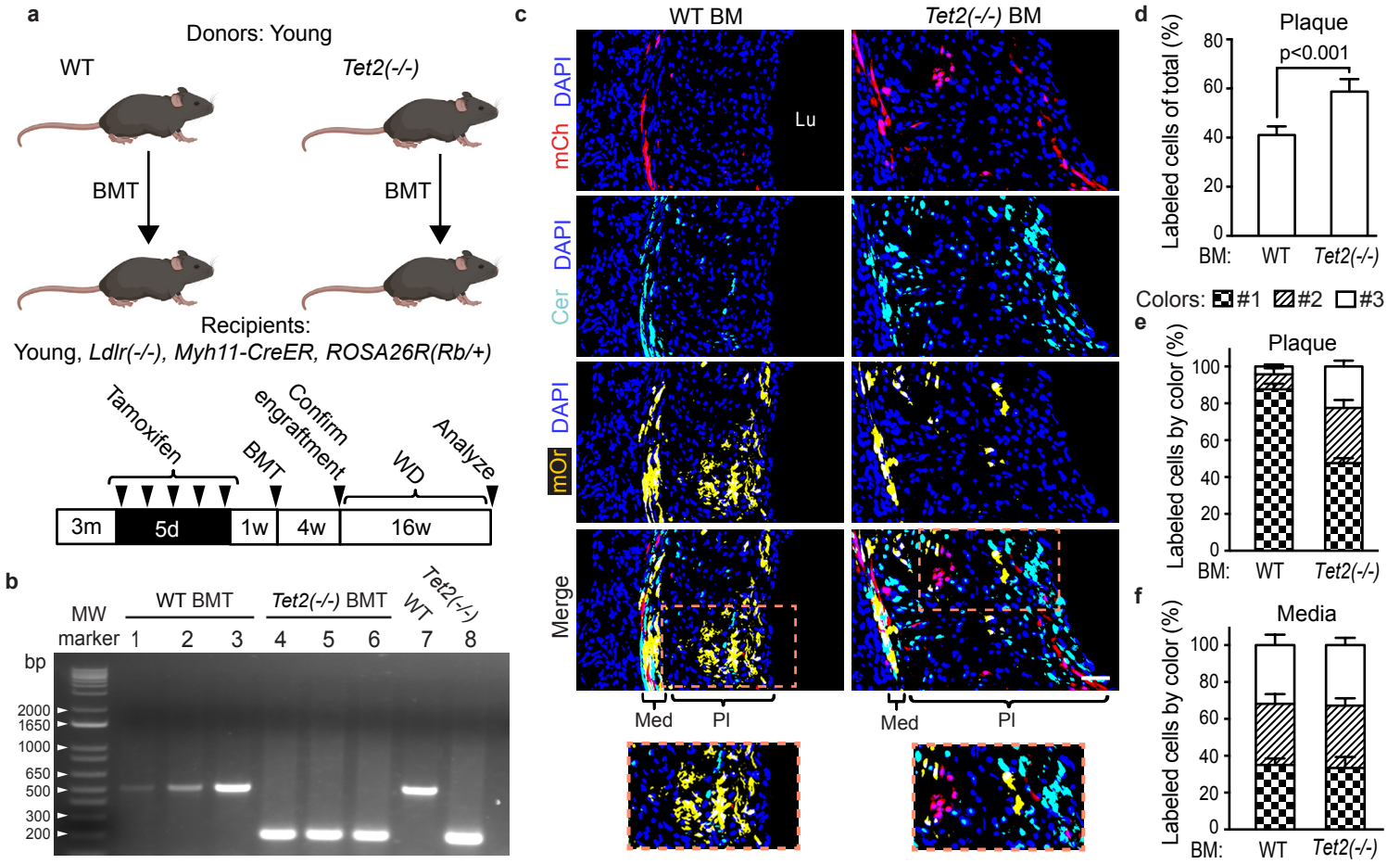

SMC culture in Mø-conditioned medium

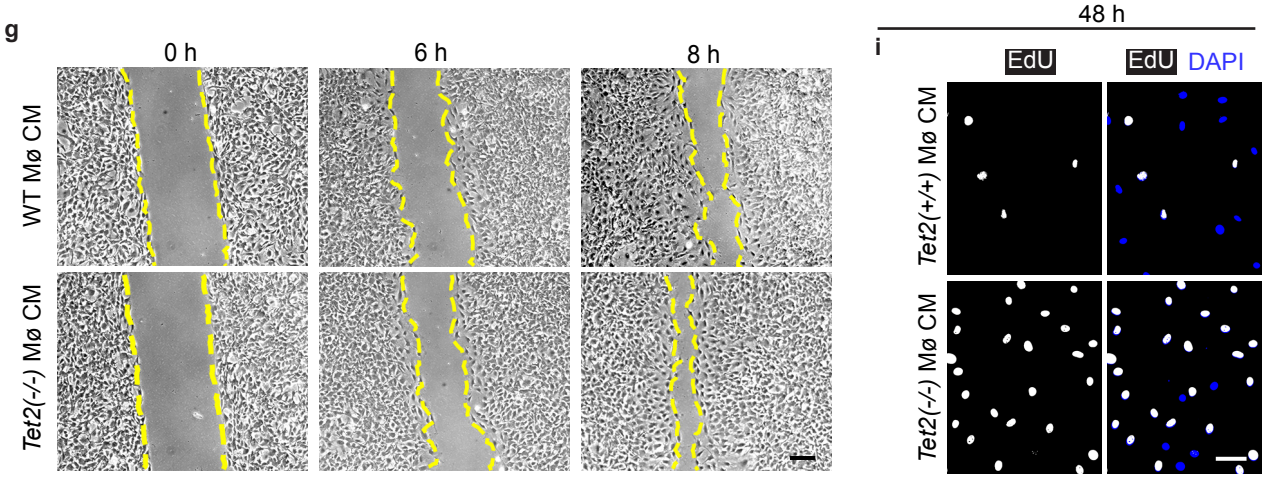

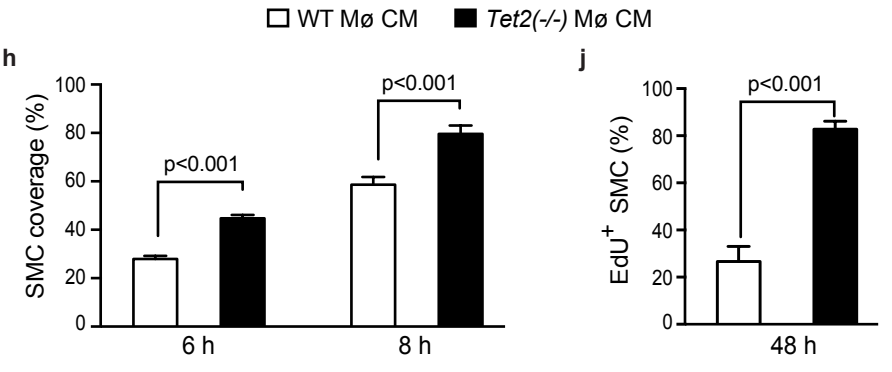

Murine Monocytes - Aged vs Young

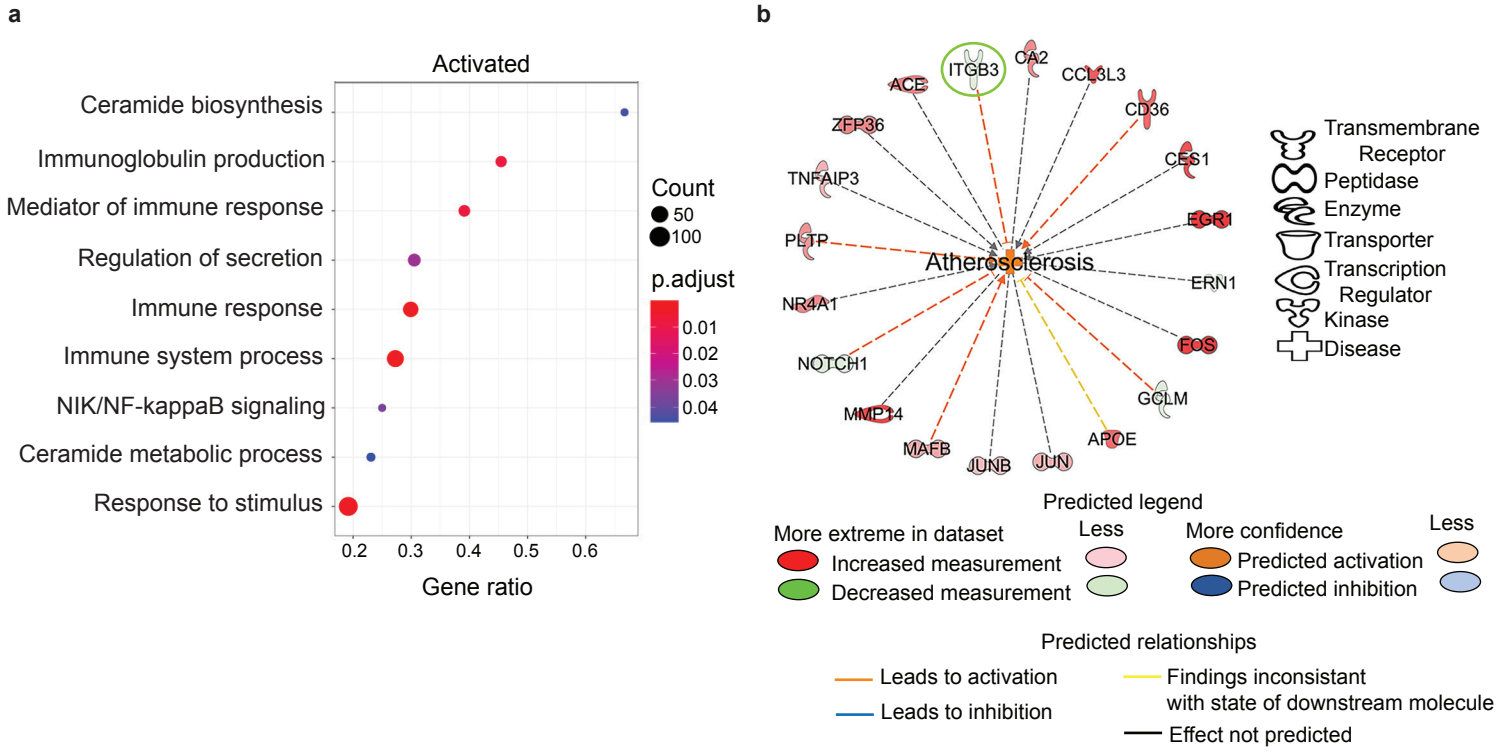

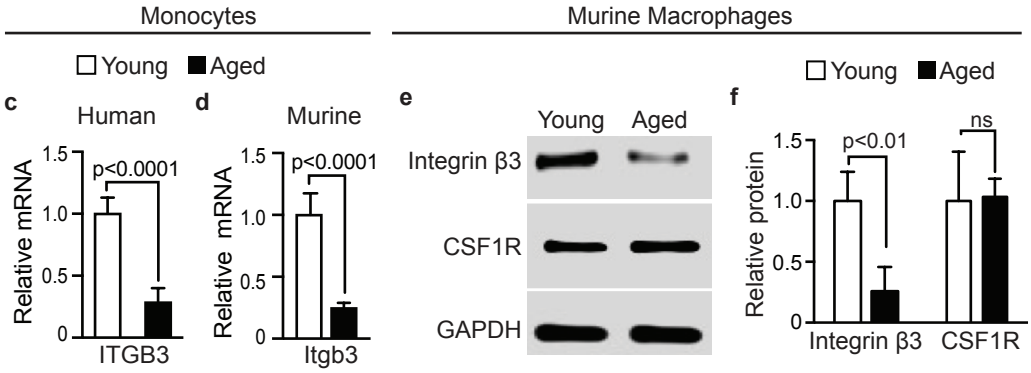

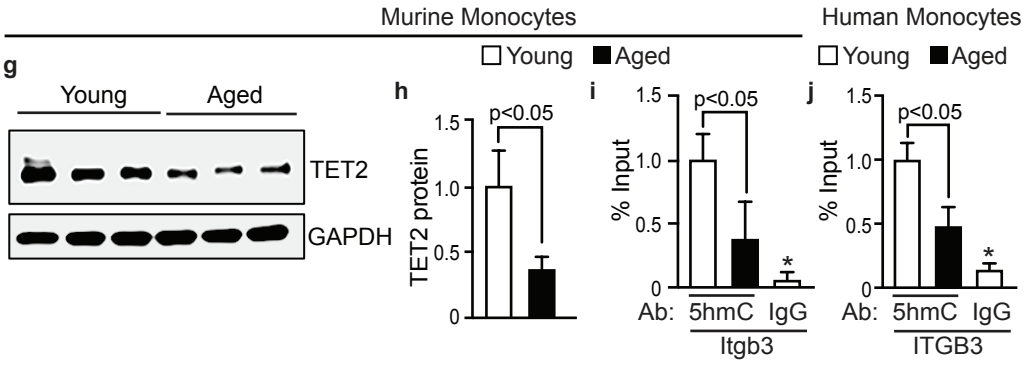

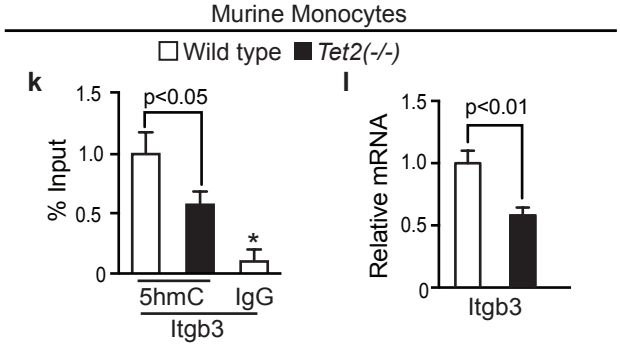

Apoe(-/-), Csf1r-Mer-iCre-Mer, WD

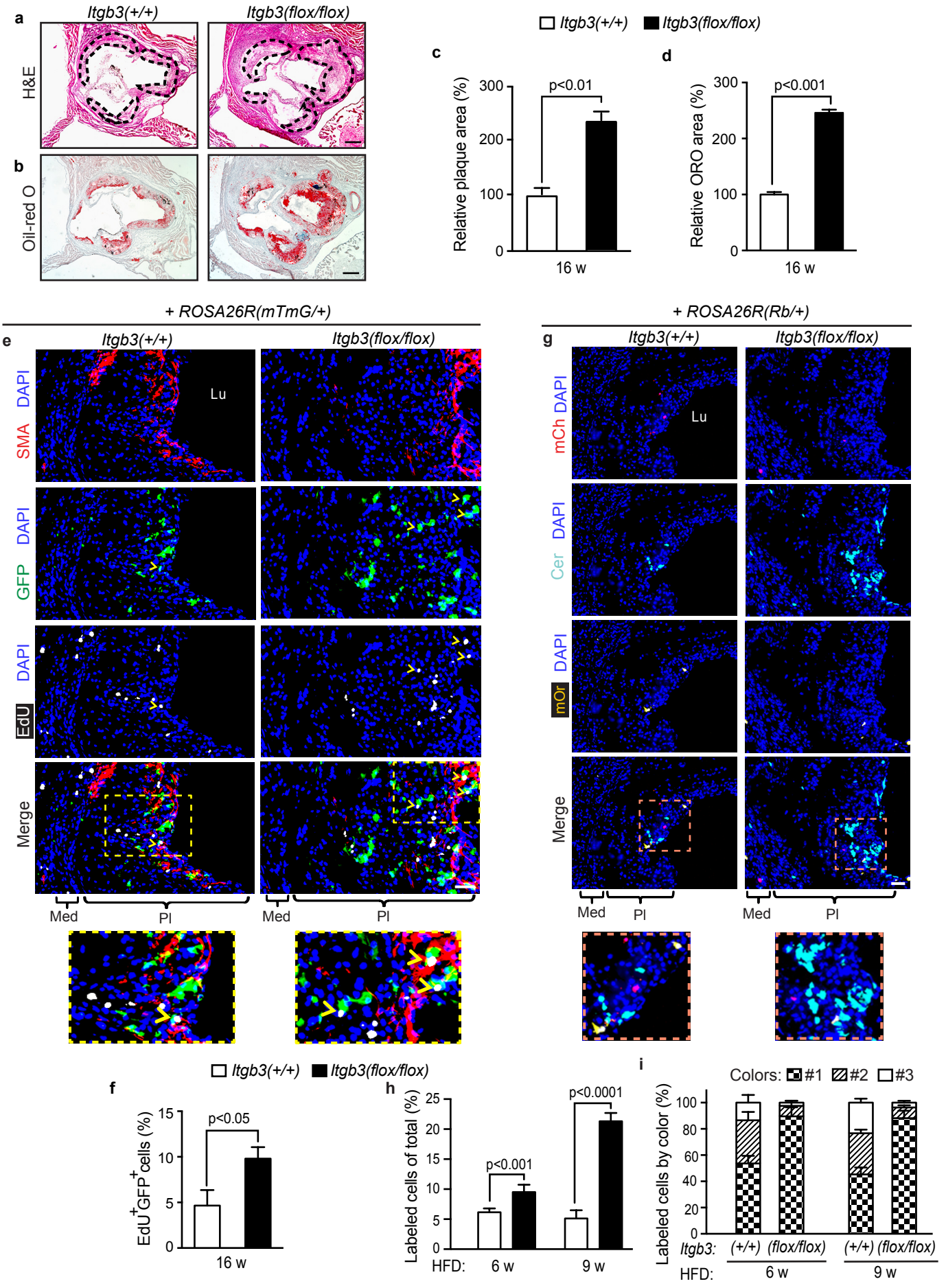

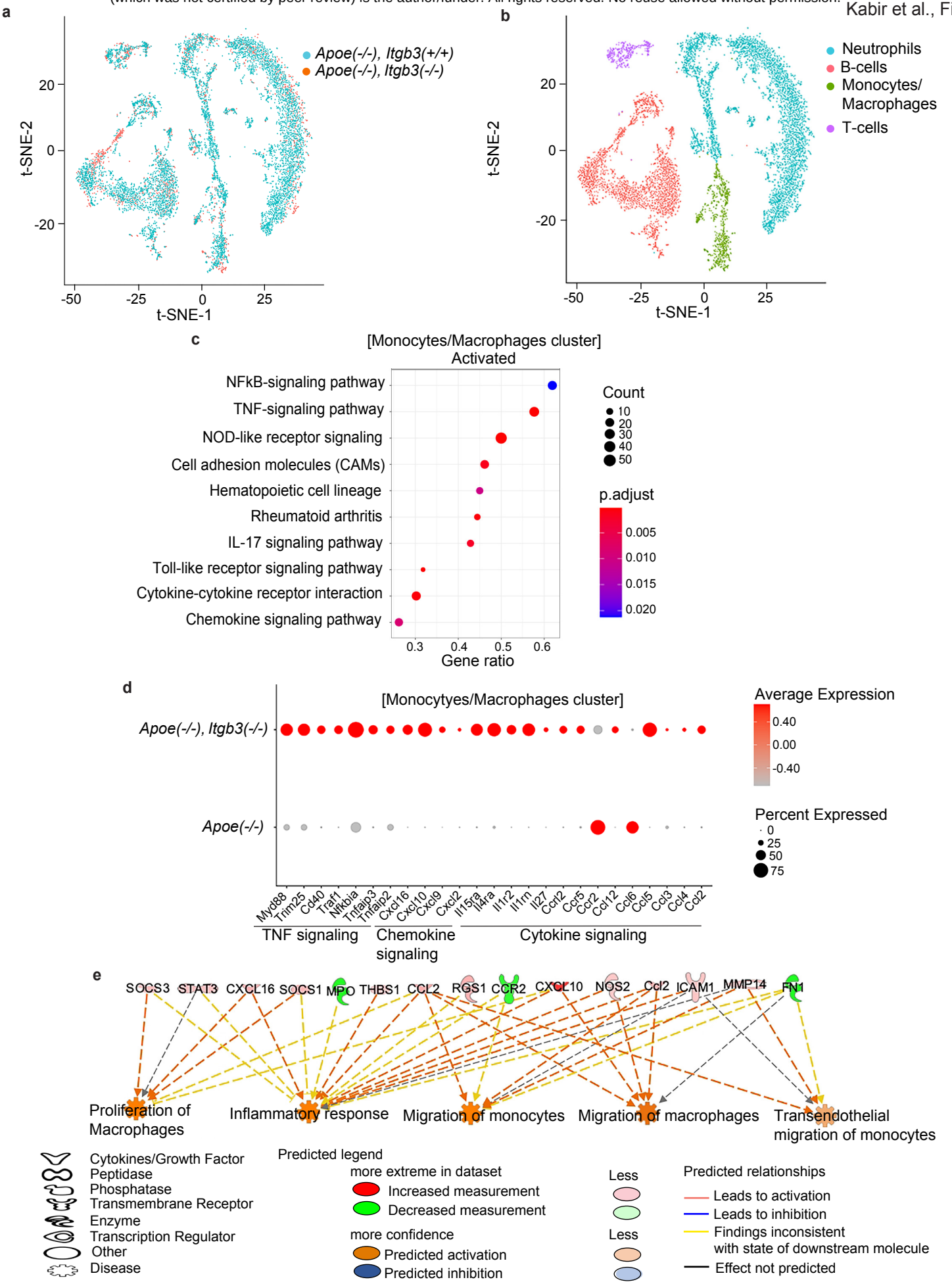

Apoe(-/-), Csf1r-Mer-iCre-Mer

Apoe(-/-), Csf1r-Mer-iCre-Mer, Itgb3(flox/flox), WD 12 Weeks

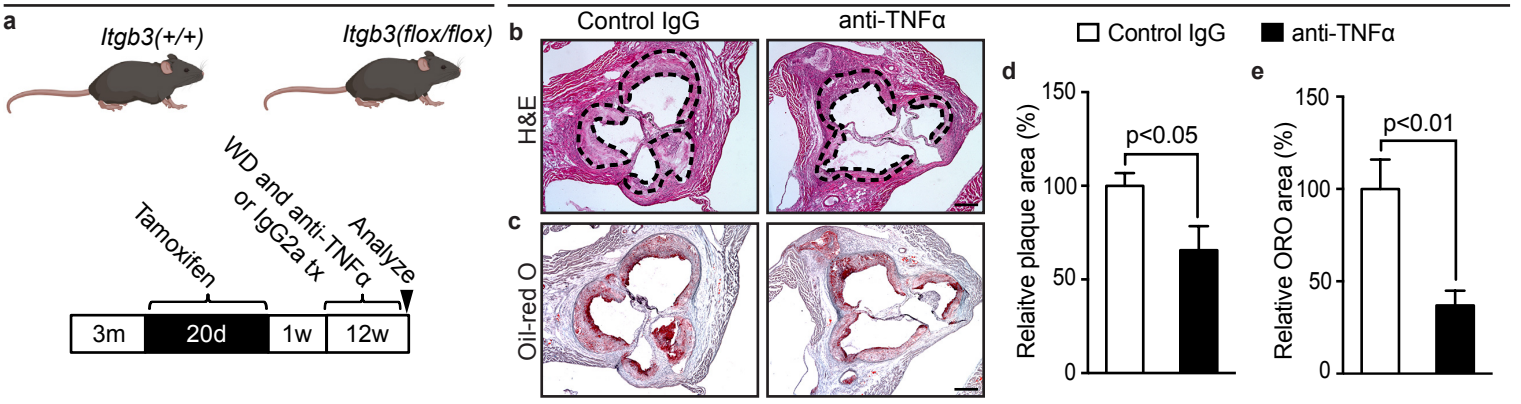

Young *Apoe(-/-), Myh11-CreER, ROSA26R(Rb/+)*, BMT, WD 12 Weeks

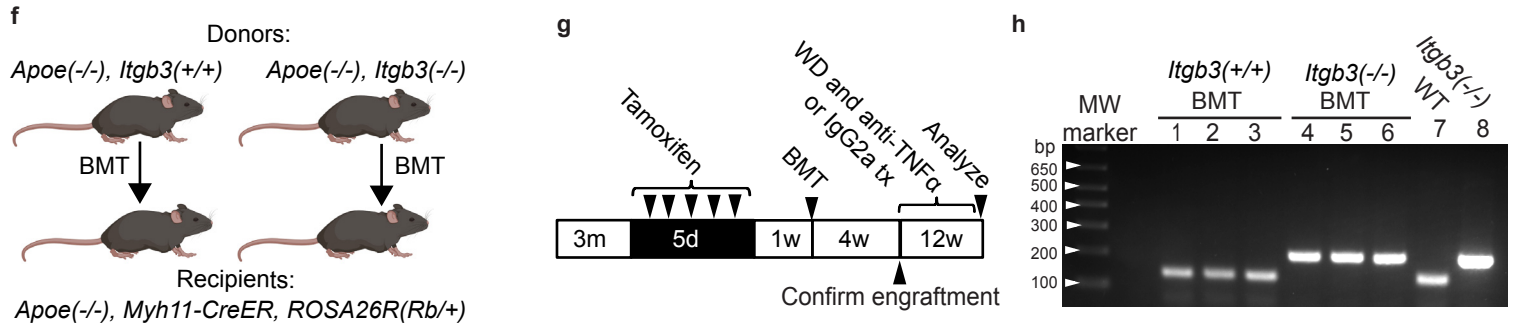

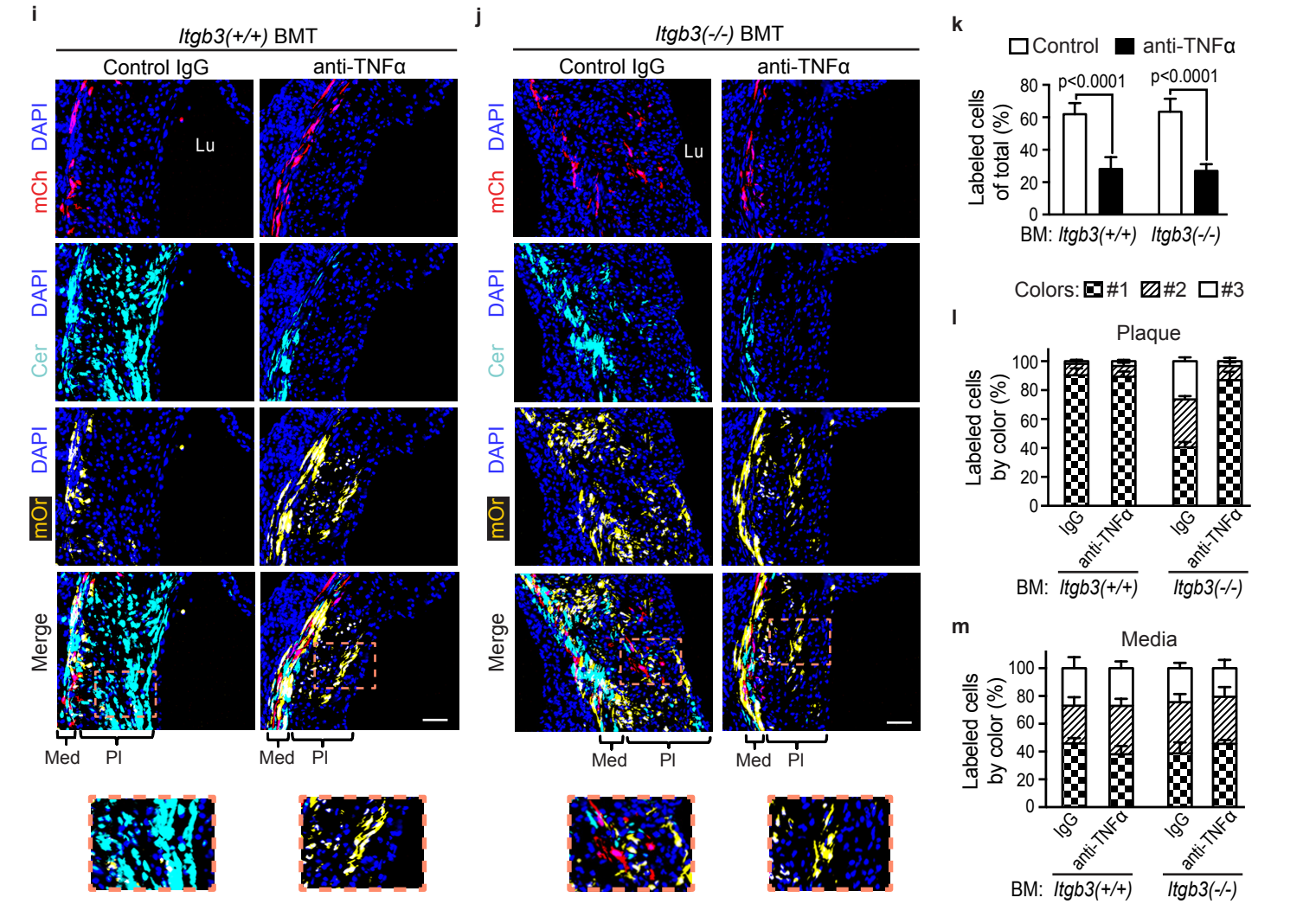

Kabir et al., Graphical Abstract